Engineering Structures 343 (2025) 120393

Contents lists available at ScienceDirect

Engineering Structures

journal homepage: www.elsevier.com/locate/engstruct

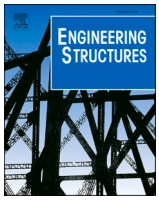

The shear design and assessment of skew reinforced concrete slabs in the new Eurocode 2

Alessandro Lipari

ENEA Italian National Agency for New Technologies, Energy and Sustainable Economic Development, SS7 Via Appia km 706, 72100 Brindisi, Italy

ARTICLE INFO

Keywords:
Concrete slabs
Skew bridges
Shear behaviour
Finite element modelling
Eurocode 2

ABSTRACT

Shear failures are generally brittle, hence highly undesired. While the shear behaviour of concrete members has been long investigated, a consensus on a model has not been reached. The recently issued second generation of Eurocode 2, EN 1992–1–1:2023, endorses a mechanical model that significantly improves the shear verification. However, it still lacks provisions readily applicable to skew slabs, common in the construction industry.

This study reviews the shear design provisions of both first and second generation of Eurocode 2, as well as relevant research on the shear design of skew concrete slabs without shear reinforcement. Procedures are then proposed to extend the Eurocode provisions to the shear design of skew slabs. Emphasis is placed on the calculation of the strains required by the new refined verification introduced in EN 1992–1–1:2023. The procedures are illustrated through the case studies of two skew railway decks. These case studies show that the second generation of Eurocode 2 returns greater design shear resistances than the first generation when using the mechanical shear span in lieu of the effective depth. However, the refined strain-based verification does not necessarily increase further the shear resistance.

1. Introduction

Considerable advances in structural codes of practice took place with the first generation of Eurocode 2, whose part 1–1 for buildings was issued in 2004 [11], in the following EC2–1:2004, and part 2 for bridges in 2005 [12], in the following EC2–2:2005. Nowadays, the Eurocodes are being developed into a second-generation suite. In 2023 the part 1–1 "General rules and rules for building, bridges and civil engineering structures" of the second generation of Eurocode 2 on the design of concrete structures, in the following EC2:2023, was issued [14], incorporating recent advances in several areas. Among those, a notable one is in the calculation of the shear resistance, which is now based on a mechanical model rather than on an empirical formulation.

Shear failures are generally brittle and, as such, highly undesirable. However, there is still no general agreement on a shear model adequately representing the behaviour of concrete members. In fact, many models have been developed to capture the shear behaviour of beams and straight slabs. Skew slabs, however, have been less investigated: whereas several numerical studies are available, there is a dearth of experimental investigations to validate the numerical findings. The early work of Cope et al. [8], as reported in Cope [6], still provides the most comprehensive experimental study on concrete skew slabs to date. They performed nine tests to failure on one-fifth scale models of solid slab bridges with skew angles of 30°, 45° and 60° subjected to dead weights and concentrated loads. The 30° and 45° skew models failed in shear with cracks in proximity of the concentrated loads and/or the support line, whereas the 60° skew model failed in punching shear around the obtuse corner bearing. It was also stated that an increasing skew angle considerably decreases the shear capacity [6]. Morrison and Weich [34] tested two quarter-scale models of a 50° skew concrete slab deck, which failed in punching shear around the obtuse corner exhibiting ductility. Miller et al. [33] tested a decommissioned 30° skew concrete slab bridge to destruction, which failed abruptly in punching shear around the loading blocks. Lantsoght et al. [27] tested a decommissioned 18° skew integral bridge, whose slab deck failed in flexure, in spite of being loaded with two concentrated loads close to the supports.

Among the numerical studies, Théoret et al. [44] proposed bending moment and shear force factors to design slab bridges with skew angles up to 60° using the equivalent beam method. Hulsebosch [18] developed a parametric tool to study the influence of various geometric parameters on skew slab bridges, which may be useful for preliminary design. Lipari [29] presented a comprehensive review of numerical and experimental studies on the shear behaviour of straight and skew slabs, and proposed procedures to extend the provisions of main codes of practice to skew slabs. Moya and Lantsoght [35] performed a parametric

E-mail address: alessandro.lipari@enea.it.

https://doi.org/10.1016/j.engstruct.2025.120393
Received 10 December 2024; Received in revised form 10 April 2025; Accepted 16 April 2025
Available online 6 August 2025

Nomenclature

A_s	effective area of tensile reinforcement
a	distance between rail support points
a_{cs}	effective shear span
a_q	edge-to-edge distance between concentrated load and support (clear distance)
$a_{s\alpha}$	area of tensile reinforcement placed at angle α from the *x*-axis per unit width
$a_{s,n}$, $a_{s,t}$	equivalent area of tensile reinforcement per unit width in *n*- and *t*-direction
$a_{s,v}$	equivalent area of tensile reinforcement per unit width in the direction of principal shear force
a_v	mechanical shear span
b_w	smallest width of the section in tensile area
c	neutral axis depth
$C_{Rd,c}$	shear factor in EC2–1:2004
D_{lower}	smallest value of upper sieve size in an aggregate
D_{max}	maximum aggregate size
d	effective depth to tensile reinforcement
d_{av}	average effective depth
d_{dg}	size parameter in EC2:2023
d_t	effective depth to transverse reinforcement
d_x, d_y	effective depth to reinforcement in *x*- and *y*-direction
E_s	modulus of elasticity of steel
$f_{s\alpha}$	force per unit width in reinforcement placed at angle α from *x*-axis
$f_{s\alpha,n}$	equivalent force per unit width in reinforcement in *n*-direction
f_{cd}, f_{ck}	design and characteristic cylinder compressive strength of concrete
f_{yd}	design yield strength of steel reinforcement
k	size effect factor in EC2–1:2004
l_{bd}	design value of anchorage length of reinforcing steel
m_{Ed}	design moment per unit width (concurrent with design shear force)
$m_{Ed,t}$	design moment per unit width along *t*-direction
$m_{Ed,x}$, $m_{Ed,y}$	design moment per unit width along *x*- and *y*-direction
$m_{Ed,xy}$	design twisting moment per unit width in *x*-*y* plane
m_n, m_t	moment per unit width along *n*- and *t*-direction
m_{nt}	twisting moment per unit width in *n*-*t* plane
m_{Rd}	design resisting moment per unit width
m_x, m_y	moment per unit width along *x*- and *y*-direction
m_{xy}	twisting moment per unit width in *x*-*y* plane
n, t	arbitrary perpendicular directions
Q_{vd}, Q_{vk}	design and characteristic value of vertical concentrated load
Q_{vi}	vertical point load on each rail (design value)
V_{Ed}	design shear force
$V_{Rd,c}$	design shear resistance
v_{Ed}	design shear force per unit width (principal shear force)
$v_{Ed,x}$, $v_{Ed,y}$	design shear force per unit width in *x*- and *y*-direction
v_{min}	minimum shear stress in EC2–1:2004
$v_{Rd,c}$	design shear resistance per unit width
z	inner lever arm
α	angle of reinforcement from *x*-axis
	adjustment factor for rail traffic load
α_v	angle of direction of principal shear force
β	factor for concentrated loads close to supports
ε_n, ε_t	strain along *n*- and *t*-direction
ε_s	strain in reinforcement
ε_v	strain at the level of tensile reinforcement in the direction of principal shear force
ε_x, ε_y	strain in reinforcement placed along *x*- and *y*-direction
γ_C	partial safety factor for concrete
γ_{def}	partial safety factor for deformations
γ_{nt}	shear strain in *n*-*t* plane
γ_Q	partial safety factor for live load
γ_V	partial safety factor for shear and punching resistance without shear reinforcement
γ_S	partial safety factor for steel
θ	angle of *n*-direction from *x*-axis
μ	ratio of transverse to longitudinal reinforcement areas
ρ	reinforcement ratio
ρ_v	equivalent reinforcement ratio in the direction of principal shear force
ρ_x, ρ_y	reinforcement ratio in *x*- and *y*-direction
$\sigma_{s\alpha}$	stress in reinforcement placed at angle α from *x*-axis
τ_{Ed}	average design shear stress over cross-section
$\tau_{Rd,c}$	design shear stress resistance
$\tau_{Rdc,min}$	minimum shear stress resistance
φ_3	railway dynamic factor

study on the applicability of the AASHTO LRFD design code [1] to simply supported skew slab bridges. They noted that AASHTO LRFD does not capture the skew effects for shear design, which can be otherwise accounted for by incorporating the recommendations made by Lipari [29] and Lantsoght et al. [24].

This shortage of studies is reflected in codes of practice, which hardly include specific provisions for skew slabs. As will be shown later, provisions for slab design were limited in EC2–1:2004 and EC2–2:2005, whereas in EC2:2023 the considerable advances introduced in the shear verification stop short of specifically addressing skew slabs. The Swiss code SIA 262 [43] is readily applicable to slabs and includes two levels of approximation, the least accurate of which is readily applicable to skew slabs. Similarly, the fib Model Codes 2010 and 2020 [19,20] also endorse an approach based on levels of approximation, whose lowest level is readily applicable to skew slabs. For further details the reader is referred to the codes or Lipari [29].

This study reviews the provisions on the shear resistance without shear reinforcement in the recent EC2:2023 and compares them with those in EC2–1:2004 and EC2–2:2005. Focus is given to skew slabs under concentrated loads close to supports, as typically occurs in bridge decks, and to the calculation of strains required in the newly introduced refined verification. Practical procedures are presented to extend the shear design principles of both Eurocode 2 provisions to skew slabs and are then applied to the design of two skew bridge decks, so as to quantify the impact of the second-generation provisions on simply supported and continuous slabs.

2. Concepts

2.1. Slabs

EC2:2023 defines a *slab* as a "planar member loaded primarily perpendicularly to its plane for which the minimum panel dimension is not less than 4 times the overall thickness" [14]. EC2–1:2004 classified a slab as *one-way spanning* when possesses two free unsupported and sensibly parallel edges *and* is subjected to dominantly uniformly distributed loads [11]. The behaviour of a one-way slab thus resembles that of a wide beam. Otherwise, slabs are said to be *two-way spanning*. It is worth noting that bridge decks are not generally subjected to dominantly uniformly distributed loads; therefore, bridge deck slabs are typically two-way spanning.

Several established methods to analyse the flexural behaviour of

slabs traditionally apply either upper or lower bound analyses from the theory of plasticity, such as those based on the *yield line theory* [23] or the *strip method* [17,46]. In the last few decades, the use of the *Finite Element Method* (FEM) has become widespread. However, the shear behaviour of concrete slabs is not quite established, particularly when no shear reinforcement is provided, as is typical in practice. Even for the simpler case of beams, there is no universal agreement on a single approach to predict the shear strength [21].

In spite of concrete being a highly non-linear material, linear elastic plate analyses provide a quick and more accurate modelling than traditional grillage or equivalent beam analyses. They can also capture the shear concentrations in the obtuse corners typical of skew slabs [7,44], without needing assumptions on the load dispersal and the associated effective width. Nevertheless, care should still be taken when interpreting shear force output in FEM-based plate analyses, as singularities, i.e., regions where the internal forces and deflections may become infinite, are likely to occur under highly concentrated loads [42]. To tackle this limitation, supports are best modelled with springs and concentrated loads should be distributed over an appropriate area as much as reasonably practicable. Whenever this is unfeasible, it must be borne in mind that an excessive mesh refinement around point supports or concentrated loads may lead to unrealistic shear forces, typically within a deck depth from the support [40]. Subsequent redistribution of forces and moments would certainly be possible [41], but this is seldom straightforward. Therefore, it remains advisable to model supports and loads as realistically as possible.

Meshing is a fundamental step in FEM-based modelling, as it strongly affects the design shear forces to be used in the subsequent verifications. The influence of many factors on meshing, among which geometry constraints, makes it difficult to give general indications. As a minimum, a mesh of quadrangular elements with sides of approximately the effective depth d and aspect ratio not greater than 2:1 should be used in the regions of interest for design or assessment. For modelling regions around supports and other discontinuities, the mesh should be locally halved or even further refined as necessary. Henze et al. [16] suggest that finite element sizes around concentrated loads should not exceed $0.5d$ or 100 mm. They also recommend using forces taken from the element centres.

It is worth noting that existing structures have likely been designed with different methods than current ones, but such methods may not necessarily be more conservative than current code prescriptions.

Slabs for bridge decks are typically parallelograms supported on opposite sides. Other uncommon shapes are not considered here, although most observations made in this study may apply. Slabs for non-integral bridges are supported either on linear supports, such as elastomeric strips, or bearings. In the latter case, a potential punching shear failure should also be checked, except for closely spaced bearings. It is worth mentioning that EC2:2023 has radically changed the punching shear resistance formulation [10] and reduced the control perimeter to $0.5d$ from the face of the supporting area.

Flexural reinforcement in slabs is typically placed according to one of the following arrangements, as shown in Fig. 1:

- Arrgt. 1: orthogonal grid with longitudinal reinforcement parallel to free edges;
- Arrgt. 2: orthogonal grid with longitudinal reinforcement perpendicular to supported edges;
- Arrgt. 3: non-orthogonal grid with longitudinal reinforcement parallel to free edges and transverse reinforcement parallel to supported edges.

In general, orthogonal arrangements should be preferred [2]. Non-orthogonal arrangements should be avoided for significantly skewed slabs, as they leave weak directions, particularly in the directions of principal moments and shear forces, resulting in a reduced efficiency. Nonetheless, non-orthogonal arrangements can be found in existing structures, due to their ease of construction.

Finally, shear reinforcement is typically avoided in slabs, as difficult to build, and codes of practice do not generally require a minimum amount, unlike for beams.

2.2. Principal shear force

From a structural 2-D analysis of a slab, two shear forces per unit width are obtained in the x- and y-axis, v_x and v_y, as well as three moments per unit width: two bending moments, m_x and m_y, and the twisting moment, m_{xy}. Fig. 2 shows the sign convention used throughout this study. Applied axial forces are not considered, as they are typically neglected in non-prestressed slabs [42].

Shear forces can be represented as vectors. The shear force acting on any direction n forming an angle θ from the x-axis, v_n, can be found from equilibrium considerations [7,30]:

$$v_n(\theta) = v_x\cos\theta + v_y\sin\theta \tag{1}$$

The *principal shear force* is crucial to analyse the shear behaviour of slabs. Its magnitude, v, and direction, α_v, are:

$$v = \sqrt{{v_x}^2 + {v_y}^2} \tag{2}$$

$$\alpha_v = \arctan\left(\frac{v_y}{v_x}\right) \tag{3}$$

Thus, the principal shear action occurs on a plane perpendicular to α_v.

Since both magnitude and direction of the principal shear forces vary across the slab, identifying the principal shear force relevant for design or assessment may not be straightforward. In the case of line or distributed loads and linear supports, the direction of the principal shear force is typically perpendicular to the support line [45]. For skew slabs,

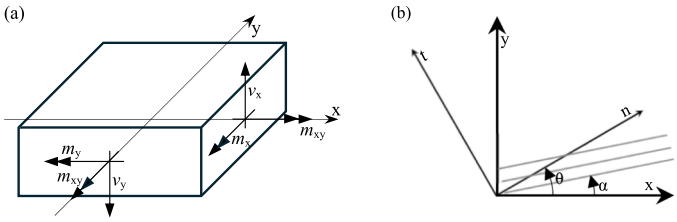

Fig. 2. Notation used: (a) shear forces and moments per unit width acting on a slab element; (b) reference axes and reinforcement orientation.

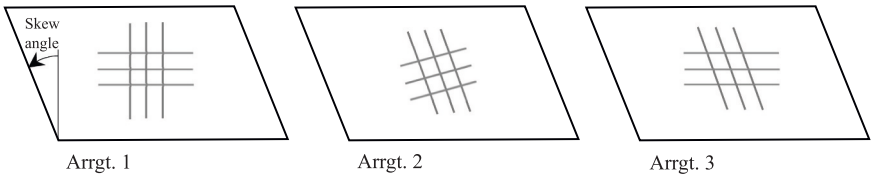

Fig. 1. Typical reinforcement arrangements for skew slabs and skew angle convention.

this implies that the direction of the principal shear force α_v is generally expected to lie at an angle roughly comparable to the skew.

In practice, a control section is often used, which is taken parallel to the support line at a certain distance from the support edge [19,25,26,41]. The control section may not necessarily coincide with the plane on which the principal shear force action occurs, i.e., perpendicular to α_v. However, the plane enclosing the control section and the plane perpendicular to α_v are expected to nearly coincide in most cases. In fact, the experiments carried out by Cope et al. [8] showed that most shear cracks in the soffit were roughly parallel to the support line [6].

2.3. Equivalent reinforcement area

The direction of the principal shear force may significantly differ from the direction of the main flexural reinforcement. This typically occurs close to the supports of skew slabs when the longitudinal reinforcement is not placed perpendicularly to the support line, like in Arrgt. 1 and 3 (Fig. 1). In such cases, the flexural reinforcement should be resolved in the direction of the principal shear force.

The concept of *equivalent reinforcement area* is useful to compute the effects of the reinforcement along any direction. With reference to Fig. 2b, the area of flexural reinforcement per unit width placed at angle α from the x-axis, $a_{s\alpha}$, may be resolved for any direction n forming an angle θ from the x-axis, $a_{s\alpha,n}$, as follows:

$$a_{s\alpha,n}(\theta) = a_{s\alpha}\cos^2(\theta-\alpha) \tag{4}$$

The $\cos^2$ function accounts for the increase in bar spacing and the decrease in effective reinforcement area per unit width with increasing angle θ. By considering multiple reinforcement layers, with index i, the overall equivalent reinforcement area, $a_{s,n}$, reads:

$$a_{s,n}(\theta) = \sum\nolimits_i a_{s\alpha_i}\cos^2(\theta-\alpha_i) \tag{5}$$

Dividing both terms for the average effective depth, d_{av}, Eq. (5) can be rewritten in terms of the reinforcement ratio, ρ:

$$\rho(\theta) = \sum\nolimits_i \rho_{\alpha_i}\cos^2(\theta-\alpha_i) \tag{6}$$

In the case of reinforcement placed along the x-y axes (Arrgt. 1, Fig. 1) and in the direction of the principal shear force ($\theta = \alpha_v$) Eqs. (5–6) simplify as:

$$a_{s,v} = a_{s,x}\cos^2\alpha_v + a_{s,y}\sin^2\alpha_v \tag{7}$$

$$\rho_v = \rho_x\cos^2\alpha_v + \rho_y\sin^2\alpha_v \tag{8}$$

Eqs. (5–8) represent mere *geometric* equivalences, giving an equivalent reinforcement area, as though an unreinforced direction were reinforced. In fact, Eqs. (5–8) underlie an assumption of yielded reinforcement, as shown by the fact that no strains are accounted for.

However, in most cases, the reinforcement is yielding under the design moment load case but it is not under the design shear load case, particularly in simply supported members, where moments close to supports are low. Therefore, it is appropriate to take the reinforcement strains into account.

In general, given any perpendicular directions n and t obtained by rotating the x-y axes by an angle θ (Fig. 2b), the normal strains along n and t, ε_n and ε_t, and the shear strain in the n-t plane, γ_{nt}, can be found as:

$$\begin{cases} \varepsilon_n(\theta) = \varepsilon_x\cos^2\theta + \varepsilon_y\sin^2\theta + \gamma_{xy}\sin\theta\cos\theta \\ \varepsilon_t(\theta) = \varepsilon_x\sin^2\theta + \varepsilon_y\cos^2\theta - \gamma_{xy}\sin\theta\cos\theta \\ \gamma_{nt}(\theta) = 2(\varepsilon_y - \varepsilon_x)\sin\theta\cos\theta + \gamma_{xy}(\cos^2\theta - \sin^2\theta) \end{cases} \tag{9}$$

Conversely, the normal strains along the x- and y-axis can be found from the strains along n and t. It will be assumed that the n-t axes nearly coincide with the principal strain directions, so that the shear strain in the n-t plane can be neglected ($\gamma_{nt} = 0$); hence:

$$\begin{cases} \varepsilon_x = \varepsilon_n\cos^2\theta + \varepsilon_t\sin^2\theta \\ \varepsilon_y = \varepsilon_n\sin^2\theta + \varepsilon_t\cos^2\theta \end{cases} \tag{10}$$

Similarly, by considering the reinforcement direction α instead of the x-axis (Fig. 2b), the reinforcement strain, $\varepsilon_{s\alpha}$, can be found as [9]:

$$\varepsilon_{s\alpha} = \varepsilon_n\cos^2(\theta-\alpha) + \varepsilon_t\sin^2(\theta-\alpha) = \varepsilon_n\left[\cos^2(\theta-\alpha) + \varepsilon_t/\varepsilon_n\cdot\sin^2(\theta-\alpha)\right] \tag{11}$$

The force per unit width in the reinforcement, $f_{s\alpha}$, when yielding is not achieved, is:

$$f_{s\alpha} = a_{s\alpha}\sigma_{s\alpha} = a_{s\alpha}E_s\varepsilon_{s\alpha} \tag{12}$$

in which $\sigma_{s\alpha}$ is the reinforcement stress and E_s the modulus of elasticity of steel. The equivalent reinforcement force per unit width along any direction n, $f_{s\alpha,n}$, can be computed from Eqs. (11–12) as:

$$\begin{aligned} f_{s\alpha,n}(\theta) &= f_{s\alpha}\cos^2(\theta-\alpha) = a_{s\alpha}E_s\varepsilon_{s\alpha}\cos^2(\theta-\alpha) \\ &= a_{s\alpha}E_s\varepsilon_n\left[\cos^4(\theta-\alpha) + \varepsilon_t/\varepsilon_n\cdot\sin^2(\theta-\alpha)\cos^2(\theta-\alpha)\right] \end{aligned} \tag{13}$$

Like in Eq. (4), the $\cos^2$ function in Eq. (13) accounts for the increase in bar spacing and the decrease in effective reinforcement area per unit width with increasing angle θ. The equivalent force $f_{s\alpha,n}$ can also be expressed in terms of an equivalent reinforcement area per unit width in the n-direction $a_{s\alpha,n}$: $f_{s\alpha,n}(\theta) = a_{s\alpha,n}(\theta)E_s\varepsilon_n$. Hence, by comparison with Eq. (13), the equivalent reinforcement area $a_{s\alpha,n}$ can be found as:

$$a_{s\alpha,n}(\theta) = a_{s\alpha}\left[\cos^4(\theta-\alpha) + \varepsilon_t/\varepsilon_n\cdot\sin^2(\theta-\alpha)\cos^2(\theta-\alpha)\right] \tag{14}$$

By considering multiple reinforcement layers i, the overall equivalent reinforcement area when strains are accounted for reads:

$$a_{s,n}(\theta) = \sum\nolimits_i a_{s\alpha_i}\left[\cos^4(\theta-\alpha_i) + \varepsilon_t/\varepsilon_n\cdot\sin^2(\theta-\alpha_i)\cos^2(\theta-\alpha_i)\right] \tag{15}$$

Inconveniently, the presence of the strain ratio ε_t / ε_n hampers the use of Eqs. (14–15), in that such strains clearly depend on the equivalent reinforcement areas along n and t. Thus, the exact equivalent reinforcement area can only be found through iterations [7].

In the case of reinforcement placed along the x-y axes (Arrgt. 1, Fig. 1) and with $\theta = \alpha_v$, Eq. (15) may be rewritten as:

$$\begin{aligned} a_{s,v} &= a_{s,x}\left(\cos^4\alpha_v + \varepsilon_t/\varepsilon_n\cdot\sin^2\alpha_v\cos^2\alpha_v\right) \\ &\quad + a_{s,y}\left(\sin^4\alpha_v + \varepsilon_t/\varepsilon_n\cdot\sin^2\alpha_v\cos^2\alpha_v\right) \\ &= a_{s,x}\left[\cos^4\alpha_v + \mu\sin^4\alpha_v + \varepsilon_t/\varepsilon_n\cdot(1+\mu)\sin^2\alpha_v\cos^2\alpha_v\right] \end{aligned} \tag{16}$$

in which μ is the ratio of the transverse to the longitudinal reinforcement areas $a_{s,y}$ / $a_{s,x}$.

Jofriet and McNeice [22] suggest that the strain ratio ε_t / ε_n can be related to the ratio ε_x / ε_y through Eq. (10), which may be useful if the reinforcement is placed along the x- and y-axis (Arrgt. 1, Fig. 1) and its strains are known:

$$\frac{\varepsilon_t}{\varepsilon_n} = \frac{\cos^2\theta - \varepsilon_x/\varepsilon_y\sin^2\theta}{\varepsilon_x/\varepsilon_y\cos^2\theta - \sin^2\theta} \tag{17}$$

Note that if ε_x / $\varepsilon_y = 1$, then ε_t / $\varepsilon_n = 1$, i.e., the strains are the same in any directions. However, if ε_x / $\varepsilon_y \neq 1$, Eq. (17) is negative around $\theta = 45°$, with a minimum value of -1 at $45°$. This implies that the equivalent reinforcement area $a_{s,v}$ (Eq. 16) tends to zero as θ approaches $45°$.

Fortunately, in the typical case of synclastic bending (ε_t / $\varepsilon_n > 0$), the ratio ε_t / ε_n in Eqs. (14–16) may be conservatively ignored and Eq. (14) may be rewritten as:

$$a_{s\alpha,n}(\theta) \approx a_{s\alpha}\cos^4(\theta-\alpha) \tag{18}$$

Eq. (18) is reasonably accurate when ε_t / $\varepsilon_n \approx 0$, for instance when a slab is cracked only in the direction perpendicular to n [5]. When this is not the case, such an approximation may prove rather conservative;

nevertheless, its use is quite practical and requires little calculation burden.

Following a derivation similar to that of Eq. (4), the overall equivalent reinforcement area and ratio for multiple reinforcement layers i can be found as [5,7,9]:

$$a_{s,n}(\theta) = \sum_i a_{s\alpha_i} \cos^4(\theta - \alpha_i) \tag{19}$$

$$\rho(\theta) = \sum_i \rho_{\alpha_i} \cos^4(\theta - \alpha_i) \tag{20}$$

In the case of reinforcement placed along the x-y axes (Arrgt. 1, Fig. 1) and with $\theta = \alpha_v$, Eqs. (19–20) simplify as:

$$a_{s,v} = a_{s,x}\cos^4\alpha_v + a_{s,y}\sin^4\alpha_v = a_{s,x}\left(\cos^4\alpha_v + \mu\sin^4\alpha_v\right) \tag{21}$$

$$\rho_v = \rho_x \cos^4\alpha_v + \rho_y \sin^4\alpha_v \tag{22}$$

Eqs. (19–22) may be regarded as effective *mechanical* equivalences, as they allow to compute the force that a fictitious reinforcement along an unreinforced direction would exercise when yielding is not achieved. Using Eqs. (19–22), rather than Eqs. (5–8), is always on the safe side.

Finally, it is worth noting that the strains in the reinforcement are often easily found and that strains in other directions n are sought, e.g., in the direction of the principal shear force. From Eq. (11), under the further assumption of synclastic bending (ε_t / ε_n > 0), ε_n can be conservatively approximated as:

$$\varepsilon_n(\theta) = \frac{\varepsilon_{s\alpha}}{\cos^2(\theta - \alpha) + \varepsilon_t/\varepsilon_n \cdot \sin^2(\theta - \alpha)} \approx \frac{\varepsilon_{s\alpha}}{\cos^2(\theta - \alpha)} \tag{23}$$

3. Shear verification in Eurocode 2

As mentioned in Section 1, the second generation of Eurocode 2 incorporates significant advances in the calculation of the shear resistance without shear reinforcement. Some main differences from the first generation are:

- the new underlying model is the mechanical-based Critical Shear Crack Theory (CSCT) [37], already implemented in the Swiss Code SIA 262 [43], rather than an empirical model [32,38];
- a new partial safety factor $\gamma_V = 1.40$ has been specifically introduced for the shear resistance of concrete members without shear reinforcement, to be used in lieu of the partial safety factor for concrete γ_C, since model uncertainties are deemed to influence the shear resistance more than material uncertainties [36];
- the shear check is now based on shear stresses ($\tau_{Rd,c} \geq \tau_{Ed}$), rather than on shear forces ($V_{Rd,c} \geq V_{Ed}$);
- two formulations are now given: a standard version in Section 8.2 to be used mainly for design, and a refined strain-based version in Annex I for assessment; note that the standard version is actually a simplification of the refined version [32,36] and that, a bit confusingly, EC2:2023 refers to both versions as “detailed verification”;
- EC2:2023 now incorporates provisions for bridges in the normative Annex K (previously given separately in EC2–2:2005).

3.1. First generation

EC2–1:2004 [11] provisions applied to ‘beam-like’ sections. The design shear resistance without shear reinforcement, $V_{Rd,c}$, reads:

$$V_{Rd,c} = C_{Rd,c} k \cdot \sqrt[3]{100\rho f_{ck}} \cdot b_w d \geq v_{min} \cdot b_w d \quad [\text{N}] \tag{24}$$

with:

$$C_{Rd,c} = \frac{0.18}{\gamma_C}$$

$$k = 1 + \sqrt{\frac{200}{d}} \leq 2.0$$

$$v_{min} = 0.035 k^{3/2} {f_{ck}}^{1/2} \ [\text{MPa}]$$

in which $\rho = A_s / b_w d \leq 0.02$, with A_s being the area of tensile reinforcement which extends at least $l_{bd} + d$ beyond the section considered; b_w is the smallest width of the section in the tensile area [mm]; d, the effective depth [mm]; f_{ck}, the characteristic cylinder compressive strength of concrete [MPa]; k, a factor which takes account of the size effect. For members subjected to predominantly uniformly distributed loading, shear forces needed not to be checked at a distance less than d from the face of the support.

EC2–1:2004 allowed shear forces due to loads applied on the upper side within a distance $0.5d \leq a_q \leq 2d$ from the edge of a support to be multiplied by a reduction factor β, provided that flexural reinforcement is fully anchored at the supports:

$$\beta = \frac{a_q}{2d} \tag{25}$$

in which a_q is the distance between the edge of the load and the edge of the support, with a minimum value $a_q = 0.5d$. This is motivated by the fact that the failure plane is steeper close to supports, which results in larger failure loads. For slabs, Lantsoght et al. [26] recommend replacing Eq. (25) with $\beta = a_q / 2.5d$, whereas Natário et al. [39] suggest $\beta = a_q / 2.75d$.

EC2–2:2005 [12] included the informative Annex LL for the design of concrete shell elements with a sandwich model, in which the outer layers (*cover*) resist membrane forces, such as axial forces and moments, and the inner layer (*core*) resists the shear forces. For the design of the inner layer, the shell element behaves like a beam in the direction of the principal shear force (Eqs. 2–3); therefore, the ‘beam-like’ design rule applied (Eq. 24) with the reinforcement ratio ρ computed as ρ_v in Eq. (8). Note that the UK National Annex to EC2–2:2005 [3] required replacing Eq. (8) with Eq. (22), as also recommended by Lipari [29].

3.2. Second generation (Section 8.2)

The design value of the shear stress resistance, $\tau_{Rd,c}$, in the standard verification of EC2:2023 Section 8.2 reads:

$$\tau_{Rd,c} = \frac{0.66}{\gamma_V} \cdot \sqrt[3]{100\rho f_{ck} \frac{d_{dg}}{d}} \geq \tau_{Rdc,min} \tag{26}$$

with:

$$d_{dg} = 16 + D_{lower} \leq 40 \text{ mm (for concrete with } f_{ck} \leq 60 \text{ MPa)}$$

$$d_{dg} = 16 + D_{lower}(60/f_{ck})^2 \leq 40 \text{ mm (for concrete with } f_{ck} > 60 \text{ MPa)}$$

$$\tau_{Rdc,min} = \frac{11}{\gamma_V} \cdot \sqrt{\frac{f_{ck}}{f_{yd}} \frac{d_{dg}}{d}}$$

in which $\rho = A_s / b_w d$, with A_s being the *effective* area of tensile reinforcement at the distance d beyond the section considered; d_{dg} is a size parameter describing the failure zone roughness; D_{lower}, the smallest value of the upper sieve size D in an aggregate for the coarsest fraction of aggregates in the concrete permitted by the specification of concrete according to EN 206 [13]; f_{yd}, the design value of the yield strength of steel. D_{lower} can be replaced by the maximum aggregate size D_{max}, if known; however, for the assessment of existing structures, it may be difficult to verify information about the aggregate size at all. Also, γ_V and other material partial safety factors may be suitably reduced according to the informative Annex A [10].

Eq. (26) implicitly assumes that the effective shear span, a_{cs}, defined as:

$$a_{cs} = \left|\frac{M_{Ed}}{V_{Ed}}\right| \geq d \tag{27}$$

is equal to $4d$ [10,38]. Indeed, for non-slender members with $a_{cs} < 4d$, the effective depth d in Eq. (26) may be beneficially replaced by the mechanical shear span, a_v:

$$a_v = \sqrt{\frac{a_{cs}}{4} d} \tag{28}$$

which, in fact, can take the values $d/2 \leq a_v < d$, thereby increasing the shear stress resistance (Eq. 26). Note that the verification using Eqs. (27–28) becomes iterative as the shear resistance depends on the applied shear force V_{Ed}. A similar iterative process is also found in the fib Model Codes 2010 and 2020 [19,20]. According to Eqs. (26–28), keeping the other parameters fixed, a bending moment M_{Ed} greater than $d \cdot V_{Ed}$ will lead to greater mechanical shear spans a_v and then to smaller shear stress resistances $\tau_{Rd,c}$.

When significant concentrated loads are applied between d and $2d$ from the face of the support, i.e., $d \leq a_q \leq 2d$, a control section located at a distance d from the face of the support should be verified. The contribution of concentrated loads applied at a clear distance $d \leq a_q \leq 2d$ to the design shear force may be reduced according to a factor equal to β of EC2–1:2004 (Eq. 25). For loads applied at a clear distance $a_q \leq d$, the shear verification of planar members on line supports may be omitted provided that the design shear stress τ_{Ed} is less than $2\tau_{Rdc,min}$ (Eq. 26) and the flexural reinforcement is fully anchored at the support. If either condition is not fulfilled, the design has to be undertaken as a discontinuity region, for instance by using strut-and-tie models. However, when $0.5d \leq a_q < d$, the contribution of the concentrated loads to the design shear forces may be multiplied by β (Eq. 25), provided that the flexural reinforcement is designed and fully anchored for the tensile force due to the concentrated load. These cases are summarised in Table 1.

In the case of distributed loads pushing against a member on the tension side, e.g., near intermediate supports, the design shear force at the control section may be reduced by ΔV_{Ed}, calculated as the sum of the distributed loads acting closer than d from the control section, but not larger than ¼ of the total contribution of the distributed load to the design shear force.

In planar members, the average shear stress over the cross-section τ_{Ed} is defined as v_{Ed} / z, in which the design shear force per unit width, v_{Ed}, should be calculated as the principal shear force (Eq. 2) and $z = 0.9d$ is the lever arm for the shear stress calculation.

The ratio of the shear forces in the y- and x-direction, $v_{Ed,y} / v_{Ed,x}$, determine whether the effective depth d is taken as the effective depth in the x- or y-axis, or else as their average, and whether the reinforcement ratio ρ is taken as the reinforcement ratio in the x- or y-axis, or else calculated as a function of the direction of the principal shear force α_v. Such rules read as follows:

- if $v_{Ed,y}/v_{Ed,x} \leq 0.5$: $d = d_x$; $\rho = \rho_x$

- if $0.5 < v_{Ed,y}/v_{Ed,x} < 2$: $d = 0.5(d_x + d_y) = d_{av}$; $\rho = \rho_x \cos^4\alpha_v + \rho_y \sin^4\alpha_v = \rho_v$ (29)

- if $v_{Ed,y}/v_{Ed,x} \geq 2$: $d = d_y$; $\rho = \rho_y$

Alternatively, the effective depth d may be taken as a function of α_v:

$$d = d_x \cos^2\alpha_v + d_y \sin^2\alpha_v \tag{30}$$

As shown in Eq. (3), the ratio of the shear forces in the y- and x-direction determines the direction of the principal shear force α_v. Hence, the thresholds $v_{Ed,y} / v_{Ed,x} = 0.5$ and 2 in Eq. (29) correspond to $\alpha_v = 26.6°$ and 64.5°. Considering that for skew slabs α_v is typically comparable to the skew angle (Section 2.2), Eq. (29) implies that slabs with skew angle less than approximately 26.6° can be designed as straight, except for the design shear force v_{Ed}, which should still be taken as the principal shear force. Note that, unlike EC2–2:2005, Eq. (29) now computes the reinforcement ratio using a $\cos^4$ function, thus implementing the recommendations in BSI [3] and Lipari [29].

Fig. 3a shows the variation of the reinforcement ratio ρ, normalised to ρ_x, with α_v (Eq. 29) and for three different ratios $\mu = \rho_y / \rho_x$. Fig. 3b shows the effects of the variation of ρ in Eq. (29) on the normalised shear stress resistance, $\tau_{Rd,c} / \sqrt[3]{f_{ck} d_{dg}/d}$. It can be seen that the effects of ρ within the thresholds $\alpha_v = 26.6°$ and 64.5°, i.e., where $\rho = \rho_v$, are not as pronounced as in Fig. 3a, but still significant.

Notably, when the shear force is not constant along the control section, EC2:2023 explicitly allows averaging over a width not larger than $2d$ on both sides from the peak of the shear force, provided that the moment equilibrium after redistribution is fulfilled. This approach accounts for the redistribution in the shear field due to cracking in bending and shear, and seems to fit the case where a peak is located near to a slab edge [38]; however, it is unclear whether the widths at each side of the peak should be the same or can differ as long as each width is not longer than $2d$. If other internal forces are applied for the calculation of the shear resistance, they may be also averaged over the same width, e.g., when calculating the effective shear span a_{cs} (Eq.27).

Finally, it should be emphasised that Eq. (29) implicitly assumes that the reinforcement is placed along the x- and y-axis (Arrgt. 1, Fig. 1). For other orthogonal grids, like Arrgt. 2, the axes may be rotated to coincide with the actual reinforcement directions. No indications are given for non-orthogonal grids, like Arrgt. 3.

Table 1
Concentrated load position and corresponding action on slabs.

Concentrated load position	Action
$a_q < 0.5d$	Shear verification may be omitted if slab on line supports; if not, design as discontinuity region
$0.5d \leq a_q < d$	Shear verification may be omitted if slab on line supports; if not, shear verification may be performed with reduced loads; if not, design as discontinuity region
$d \leq a_q \leq 2d$	Shear verification with reduced loads and control section located at d from support face
$a_q > 2d$	Shear verification with full loads

3.3. Second generation (Annex I)

The design value of the shear stress resistance of members without shear reinforcement in the refined verification included in the informative Annex I "Assessment of Existing Structures" (Section I.8.3) reads:

$$\tau_{Rd,c} = 0.33 \frac{\gamma_{def}^{2/3}}{\gamma_V^2} \frac{\sqrt{f_{ck}}}{1 + 24\gamma_{def}\varepsilon_v \frac{d_{dg}}{d}} \tag{31}$$

in which $\gamma_{def} = 1.33$ is a partial safety factor which covers the uncertainties related to the calculation of the deformation and ε_v the strain in the longitudinal tensile reinforcement. Such strain should be calculated according to the typical assumptions made for determining the ultimate moment resistance, i.e., plane sections remain plane, tensile strength of concrete ignored. The strain refers to the direction of the principal shear force α_v and implicitly considers the effects of the mechanical shear span a_v (Eq. 28), which should then not be used for this verification. Strains may be derived from a non-linear cross-sectional analysis and the obtained internal forces averaged over the same width mentioned in Section 3.2. Notably, the control section should be located not closer than $d/2$ from a support, concentrated load or discontinuity. However, obtaining realistic shear force values from FEM-based analyses at such a short distance may prove problematic (see Section 2.1).

When the reinforcement grid is orthogonal and does not significantly deviate from the direction of the principal shear force, as expected in

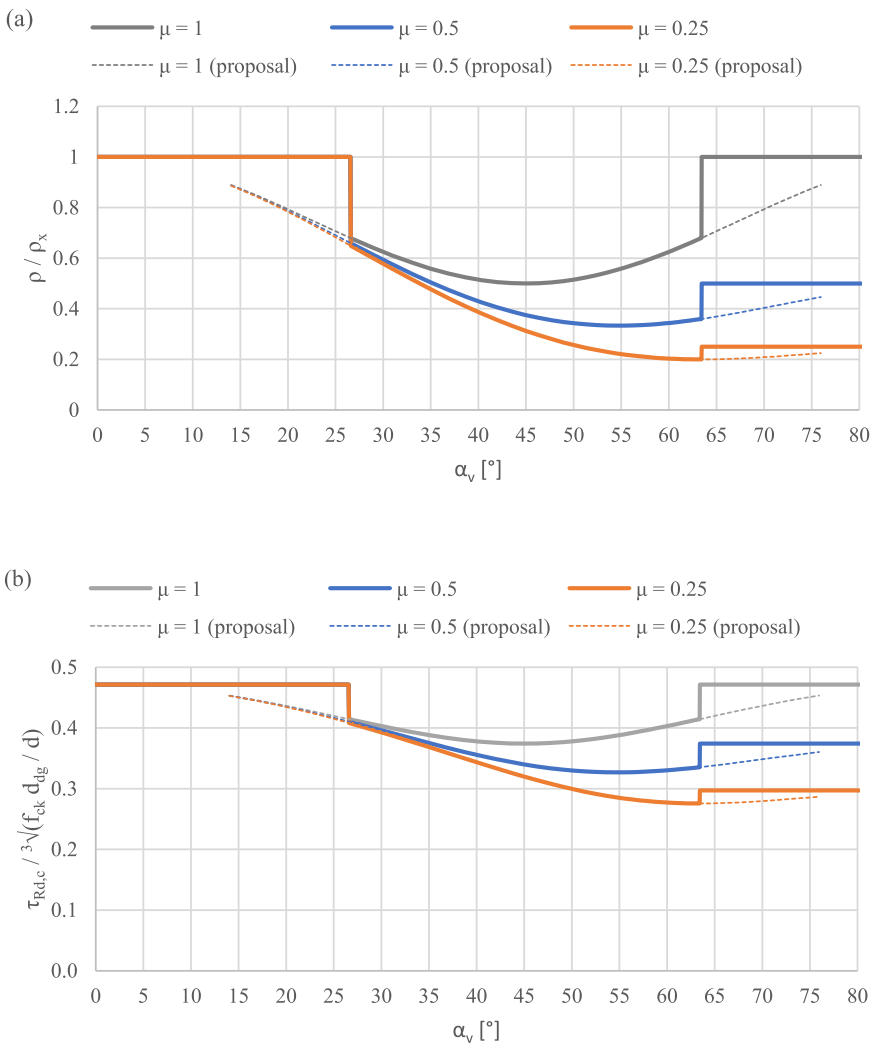

Fig. 3. Variation of (a) equivalent reinforcement ratio and (b) normalised shear stress resistance, with direction of principal shear force (full lines as per EC2:2023, dashed lines as proposed in Section 4.2 below).

Arrgt. 2 (Fig. 1), the application of the refined verification for skew slabs only requires retrieving the strain from a cross-sectional analysis. Regrettably, Annex I does not prescribe how to deal with significant deviations of the principal shear force from the longitudinal reinforcement. The designer/assessor is then left with the burden of finding the strains in a direction along which no reinforcement is placed.

4. Procedures for skew slabs

4.1. First-generation verification

The EC2–1:2004 verification should be simply performed considering shear forces per unit width in the direction of the principal shear force α_v. As such, the main modifications in Eq. (24) consist of considering a unit width and using the equivalent reinforcement ratio in the direction of the principal shear force ρ_v. The latter should be computed according to either the general Eq. (20) or Eq. (22), as suggested in Lipari [29], in lieu of the less conservative Eq. (6) or Eq. (8). For Arrgt. 2 (Fig. 1), it is convenient to rotate the local *x*-*y* axes, so that the *x*-axis lies along the longitudinal reinforcement. i.e., perpendicular to supports.

4.2. Second-generation verification (Section 8.2)

For the standard verification in EC2:2023 Section 8.2, the check with orthogonal reinforcement grids (Arrgt. 1 and 2, Fig. 1) does not pose particular issues, other than taking values of moments and shear forces per unit width if the effective shear span a_{cs} is considered, i.e., using m_{Ed} and v_{Ed} in Eq. (27). Again, for Arrgt. 2, it is convenient to rotate the local *x*-*y* axes, so that the *x*-axis lies along the longitudinal reinforcement.

However, since there is sufficient evidence that the behaviour of significantly skewed slabs differs considerably from that of straight slabs [6,18,29,35,44], it is recommended here that the thresholds in Eq. (29) be modified as follows:

$$\begin{aligned}
&\text{- if } v_{Ed,y}/v_{Ed,x} \le 0.25\text{: } v_{Ed} = v_{Ed,x};\ d = d_x;\ \rho = \rho_x \\
&\text{- if } 0.25 < v_{Ed,y}/v_{Ed,x} < 4\text{: } v_{Ed} = \sqrt{{v_{Ed,x}}^2 + {v_{Ed,y}}^2};\\
&\qquad d = 0.5(d_x + d_y) = d_{av};\ \rho = \rho_x \cos^4\alpha_v + \rho_y \sin^4\alpha_v = \rho_v \\
&\text{- if } v_{Ed,y}/v_{Ed,x} \ge 4\text{: } v_{Ed} = v_{Ed,y};\ d = d_y;\ \rho = \rho_y
\end{aligned} \tag{32}$$

Alternatively, the average effective depth d_{av} can be taken as a function of α_v (Eq. 30).

Eq. (32) means that simplifications cannot be applied when α_v is between approximately 15° and 75°. The extensions proposed for the reinforcement ratio $\rho = \rho_v$ in Eq. (32) are plotted, normalised to ρ_x, as dashed lines in Fig. 3a. Their effects on the normalised shear stress resistance are plotted in Fig. 3b.

Furthermore, a simplification is introduced in Eq. (32). Indeed, for very small and very large angles, the check may be entirely performed

along the *x*- or *y*-axis by using respectively the design shear forces $v_{Ed,x}$ or $v_{Ed,y}$, since in these cases the principal shear force v_{Ed} is typically marginally greater than $v_{Ed,x}$ or $v_{Ed,y}$.

Finally, Eq. (32) may be generalised to non-orthogonal grids with longitudinal reinforcement placed along the *x*-axis and transverse reinforcement at an angle α_t from the *x*-axis (Arrgt. 3, Fig. 1) as follows:

$$\begin{aligned}&\text{- if } v_{Ed,y}/v_{Ed,x} \le 0.25\text{: } v_{Ed} = v_{Ed,x};\ d = d_x;\ \rho = \rho_x\\&\text{- if } v_{Ed,y}\Big/v_{Ed,x} > 0.25 : v_{Ed} = \sqrt{{v_{Ed,x}}^2 + {v_{Ed,y}}^2};\ \ d = d_x\cos^2\alpha_v + d_t\sin^2\alpha_v;\ \rho \\&\qquad\qquad = \rho_x\cos^4\alpha_v + \rho_t\cos^4(\alpha_v - \alpha_t)\end{aligned} \tag{33}$$

in which d_t and ρ_t are the effective depth and the reinforcement ratio of the transverse reinforcement.

4.3. Second-generation verification (Annex I)

The refined verification in EC2:2023 Annex I requires knowledge of the strain in the tensile reinforcement ε_v. This is straightforward when the reinforcement lies approximately along the direction of the principal shear force, as expected in Arrgt. 2 (Fig. 1). Otherwise, for Arrgt. 1 and 3, the strain has to be found at the level of the reinforcement, but in a direction along which no reinforcement is placed, typically that of the principal shear force α_v. Therefore, in the following it is understood that ε_v is the strain required by the refined verification, even though it may not coincide with the actual reinforcement strain.

4.3.1. Options for strain calculation for reinforcement arrangements 1 and 3

In this section, five options to find the strain ε_v from the strain in the longitudinal reinforcement ε_x are proposed for Arrgt. 1 and 3 (Fig. 1). The strain ε_x can be calculated using the typical assumptions outlined in Section 3.3, as also suggested in EC2:2023. The options assume the common case of bending reinforcement in an elastic state and consider the direction of the principal shear force ($\theta = \alpha_v$).

Option 1. Compute the strains ε_v from Eq. (23) with $\varepsilon_t = 0$:

$$\varepsilon_v = \frac{\varepsilon_x}{\cos^2\alpha_v} \tag{34}$$

Option 2. Apply to the reinforcement strain ε_x the factor $1 / [\sin^4(\alpha_v - \alpha_l) + \cos^4(\alpha_v - \alpha_l)]$ prescribed in SIA 262 when the direction of the principal shear force α_v significantly deviates from that of the main reinforcement, α_l [43]. In the present case of Arrgt. 1 and 3, the main reinforcement is along the *x*-axis ($\alpha_l = 0$); hence:

$$\varepsilon_v = \frac{\varepsilon_x}{\sin^4\alpha_v + \cos^4\alpha_v} \tag{35}$$

Option 3. First, compute an equivalent reinforcement area $a_{s,v}$ from either the general Eq. (5) in the direction of the principal shear force (Arrgt. 3) or Eq. (7) (Arrgt. 1). Then, find the *resisting* moment m_{Rd} by means of a cross-sectional analysis or else of approximated formulae based on the theory of plasticity [37]. Finally, compute strains as proportional to the bending utilization according to SIA 262 [43]:

$$\varepsilon_v = \frac{f_{yd}}{E_s}\frac{m_{Ed}}{m_{Rd}} \approx \frac{|m_{Ed}|}{E_s a_{s,v} d f_{yd}\left(1 - \frac{a_{s,v} f_{yd}}{2 d f_{cd}}\right)} \tag{36}$$

Clearly, the applied bending moment m_{Ed} is that concurrent with the principal shear force v_{Ed} and needs to be resolved along its direction α_v, which can be done by equilibrium:

$$m_{Ed} = m_{Ed,x}\cos^2\alpha_v + m_{Ed,y}\sin^2\alpha_v + 2m_{Ed,xy}\cos\alpha_v\sin\alpha_v \tag{37}$$

Note that, since the equivalent reinforcement area $a_{s,v}$ in Eq. (36) is used for a ULS analysis, the reinforcement is expected to yield (*under-reinforced section*) and $a_{s,v}$ must be consistently computed from the general Eq. (5) or Eq. (7). Notably, Eq. (36) does not require any assumptions on the principal strain directions or the cracking state of the slab.

Option 4a. First, compute an equivalent reinforcement area $a_{s,v}$ either from the general Eq. (19) in the direction of the principal shear force (Arrgt. 3) or Eq. (21) (Arrgt. 1). The strain ε_v can be then found by equilibrium under the assumption of linear elastic behaviour of the tensile reinforcement [4,32,38]:

$$\varepsilon_v = \frac{|m_{Ed}|}{z E_s a_{s,v}} = \frac{|m_{Ed}|}{E_s a_{s,v}(d - c/3)} \approx \frac{|m_{Ed}|}{0.9 E_s a_{s,v} d} \tag{38}$$

in which the lever arm z can be found through computation of the neutral axis depth, c, or else approximated as $z = 0.9d$. The latter is used in the following, as also indicated in EC2:2023.

Option 4b. If the strains in the *t*-direction ε_t, i.e., perpendicular to the principal shear force, are significant and in the typical case of synclastic bending, that is $\varepsilon_t / \varepsilon_v > 0$, then the strain ε_v from Option 4a can be refined. If so, compute the strain ε_t, which can be found similarly to Eq. (38):

$$\varepsilon_t = \frac{|m_{Ed,t}|}{z E_s a_{s,t}} = \frac{|m_{Ed,t}|}{E_s a_{s,t}(d - c/3)} \approx \frac{|m_{Ed,t}|}{0.9 E_s a_{s,t} d} \tag{39}$$

in which the equivalent reinforcement area in the *t*-direction, $a_{s,t}$, is found from Eq. (19) with $\theta = \alpha_v + 90°$, and the applied moment in the same direction, $m_{Ed,t}$, is found from equilibrium:

$$m_{Ed,t} = m_{Ed,x}\sin^2\alpha_v + m_{Ed,y}\cos^2\alpha_v - 2m_{Ed,xy}\cos\alpha_v\sin\alpha_v \tag{40}$$

Then, compute the ratio $\varepsilon_t / \varepsilon_v$ to find a refined value of the equivalent reinforcement area $a_{s,v}$ from Eq. (15) with $\theta = \alpha_v$. Finally, use the refined value of $a_{s,v}$ to find a more refined value of ε_v from Eq. (38). In fact, this option corresponds to performing one iteration step towards the exact value of the strain ε_v.

Option 5. If the reinforcement is placed along the *x*- and *y*-axis (Arrgt. 1, Fig. 1), compute the strain ratio $\varepsilon_x / \varepsilon_y$ from cross-sectional analyses. Then, find the ratio $\varepsilon_t / \varepsilon_v$ from Eq. (17) and the equivalent reinforcement area $a_{s,v}$ from Eq. (16). Finally, compute ε_v from Eq. (38).

To sum up, Options 1–4 can be applied to non-orthogonal grids (Arrgt. 3, Fig. 1). In particular, Options 1 and 2 do not depend on the transverse reinforcement, so they would return identical results for Arrgt. 1 and 3. Options 3 and 4 can be adapted to either reinforcement arrangement by using the appropriate equivalent reinforcement area $a_{s,v}$, as described above.

4.3.2. Testing the options for strain calculation

In order to test the options proposed in Section 4.3.1, let us assume an orthogonal reinforcement grid along the *x*-*y* axes (Arrgt. 1, Fig. 1) and consider the variation of the strain ratio $\varepsilon_n / \varepsilon_x$ for different angles θ (*n*-direction, Fig. 2b), which may correspond to the direction of the principal shear force α_v.

Fig. 4 shows Options 1 and 2, as well as Option 3 for three different ratios of transverse to longitudinal reinforcement areas, μ. Option 3 assumes that the bending utilisation is the same in both longitudinal and transverse directions, i.e., $m_x / m_{R,x} = m_y / m_{R,y}$, and that applied twisting moments m_{xy} are equal to m_y and zero. As can be seen, Option 3 is rather sensitive to the amount of twisting moment m_{xy}: the smaller the twisting moments, the flatter the curves of the strain ratio. It is worth noting that twisting moments are expected to be more significant for greater skew angles.

Fig. 5 shows Options 4 and 5 when $\mu = 1$ (isotropic reinforcement), along with the same Options 1 and 2 depicted in Fig. 4. Options 4 and 5 assume that $m_n = m_t$ and $m_{nt} = 0$, i.e., all directions are principal, since the absence of shear strain is the main assumption underlying these options. As a result, $\varepsilon_t / \varepsilon_n = 1$ throughout and Option 5 is exact without any need of computing $\varepsilon_x / \varepsilon_y$; also, $m_x = m_y = m_n = m_t$ and $m_{xy} = m_{nt}$

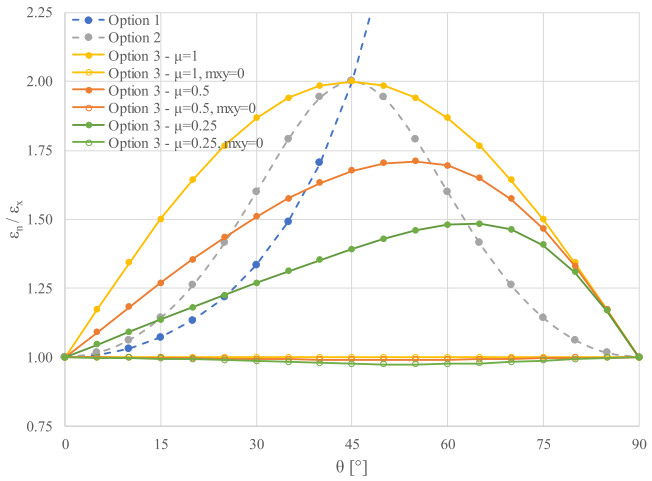

Fig. 4. Options 1, 2, 3 for strain calculation.

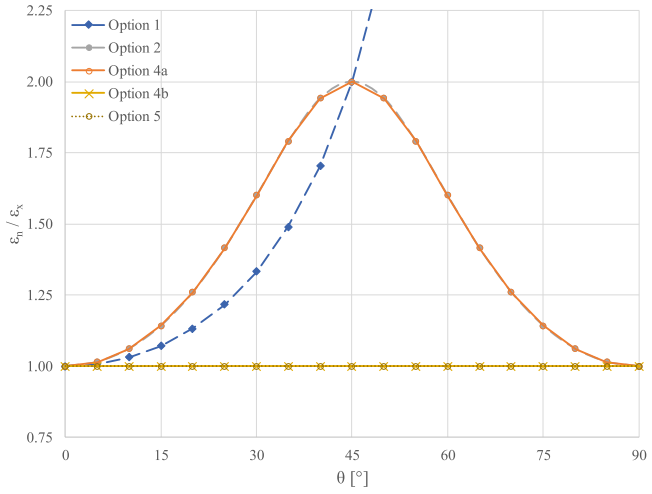

Fig. 5. Options 1, 2, 4, 5 for strain calculation with $\mu = 1$.

$= 0$. In this case, Option 4a corresponds to the function given in SIA 262 (Option 2), returning at most twice as large strains ε_n as the reinforcement strain ε_x, and Option 4b is identical to Option 5. The trends of Options 4 accord to Lenschow and Sozen [28].

In contrast, the trends are quite different when the reinforcement is not isotropic, as shown in Fig. 6 for $\mu = 0.5$. Fig. 6a assumes $m_n = m_t$ and $m_{nt} = 0$, consistently with the assumptions made for $\mu = 1$. However, in this case, the strains in the *n*- and *t*-direction are not equal throughout due to the different amounts of reinforcement. Seven exact strain ratio values $\varepsilon_v / \varepsilon_x$ are computed iteratively and plotted as benchmark, resulting in equal or close values to Option 4b (within ±10%). It can be noticed that strains are generally larger than in Fig. 5 and mostly overestimated, and that Option 5 has a very different trend from the others. Also, for certain directions, the strains ε_n can be smaller than the reinforcement strain ε_x ($\varepsilon_n / \varepsilon_x < 1$). The trends of Options 4 again accord to Lenschow and Sozen [28].

Fig. 6b assumes a more realistic moment field for moderately skewed slabs: $m_x = 2m_y = 2m_{xy}$. This means that only one direction is principal; therefore, some inaccuracies may be found. The strain ratio in the principal moment direction ($\theta = 31.7°$) is plotted for reference and falls within the trend of Option 4b. Options 2 and 5 underestimate the strains, whereas Option 4a overestimate them. It must be noted that the curves of Options 4 and 5 would become flatter if twisting moments reduced.

To sum up, Options 1 and 2 are easy to compute but can return

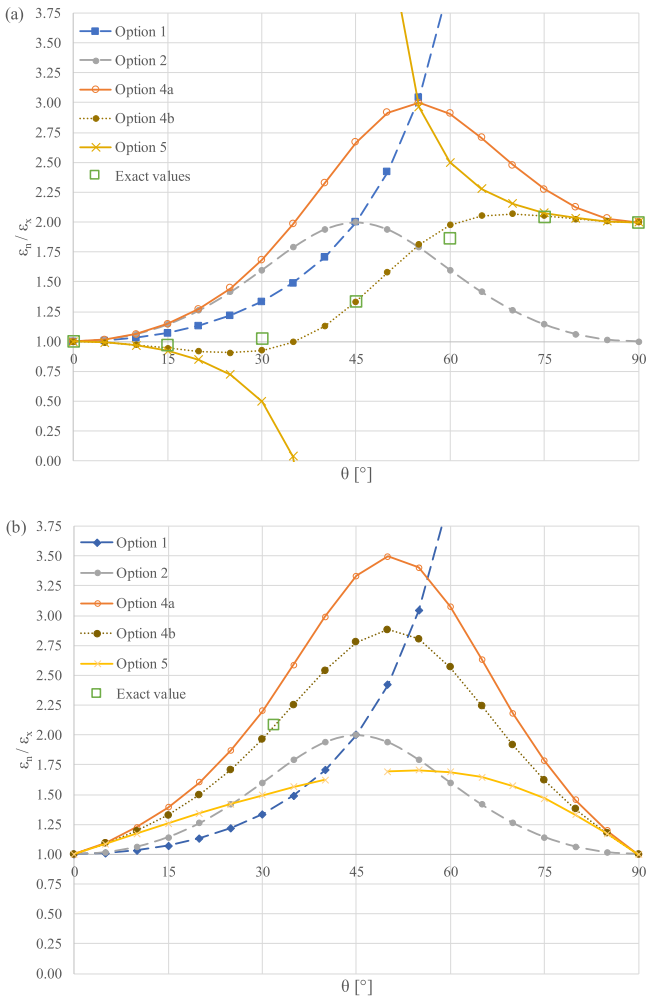

Fig. 6. Options 1, 2, 4, 5 for strain calculation with $\mu = 0.5$: (a) $m_n = m_t$; (b) $m_x = 2m_y = 2m_{xy}$.

unsafe values at times. Option 1 gives lower values than Option 2 below 45° and should not be used for skew angles greater than 45°. Option 2 is not recommended with large differences between longitudinal and transverse reinforcement ($\mu \ll 1$), as may occur in bridge decks, and with large twisting moments. Option 4a can overestimate strains but is generally the safest option to use, at the cost of a modest computation effort. Option 5 can be quite misleading, so its use is not recommended. Option 4b is the most accurate, as it quickly tends to the exact strain values, even with a single iteration step.

Finally, it is worth noting that the slab may be uncracked under moments concurrent with the design shear force, which results in limited reinforcement strains. It is then conservative to use the typical assumption of cracked concrete, i.e., ignoring its tensile strength, when considering the direction of the principal shear force (*n*-direction), as this leads to greater reinforcement strains. However, an assumption of cracked concrete may be slightly non-conservative when considering the direction perpendicular to the principal shear force (*t*-direction), like in Option 4b. Indeed, ignoring the concrete tensile strength in the *t*-direction will lead to a greater equivalent reinforcement area through the strain ratio $\varepsilon_t / \varepsilon_n$ in Eqs. (14–16), although such an overestimation is not expected to have large effects on the shear stress resistance. In fact, whenever it is possible to ascertain that concrete is uncracked in the *t*-direction, i.e., $\varepsilon_t \approx 0$, it is appropriate to use Option 4a, since it is derived under the assumption $\varepsilon_t / \varepsilon_n = 0$.

5. Case studies

In this section, the procedures for skew slabs illustrated in Section 4 are applied to two skew railway bridge decks. These case studies enable the comparison of the shear resistance in proximity to an end (simply supported slab) and an intermediate support (continuous slab).

The decks are modelled in the FEM-based software *MIDAS Civil* with quadrangular thick plate elements, which account for shear deformations by means of the Mindlin-Reissner theory [31].

The applied rail traffic load is the Load Model 71 (LM71) according to Eurocode 1 part 2 [15] (Fig. 7a). The design axle load at ULS, Q_{vd}, is:

$$Q_{vd} = \gamma_Q \alpha \varphi_3 \cdot Q_{vk} \tag{41}$$

in which γ_Q is the partial safety factor for rail traffic actions; α, the adjustment factor; φ_3, the dynamic factor for standard maintenance; Q_{vk}, the characteristic value of the concentrated load (Fig. 7a). In Eq. (41), $\gamma_Q = 1.45$ and $\alpha = 1.21$ are used. The point loads on each rail, $Q_{vi} = Q_{vd}/2$, are distributed longitudinally over three rail support points, as allowed in Eurocode 1 part 2, with $a = 0.65$ m (Fig. 7b). No other distributions of point loads, such as by sleepers and ballast, are accounted for.

The location of the LM71 should be carefully chosen. Typically, the maximum design shear force is found by placing the LM71 so that the largest point load $Q_{vi}/2$ lies at a distance of approximately $2d$ from the support edge ($a_q \approx 2d$). In fact, while a concentrated load closer than $2d$ to the supports would generally increase the shear forces [16], the contribution of such load to the shear forces should be reduced (Table 1) and this latter reduction effect on shear forces is typically dominant over the former increase effect.

The above consideration suffices for the EC2–1:2004 verification, as well as for the EC2:2023 Section 8.2 verification when using the effective depth d. In contrast, when using the mechanical shear span a_v, the effect of m_{Ed} / v_{Ed} on the shear stress resistance $\tau_{Rd,c}$ at the control section (Eqs. 26–28) should also be considered, so as to find the load location leading to the greatest shear utilisation τ_{Ed} / $\tau_{Rd,c}$. Furthermore, for the refined verification of EC2:2023 Annex I, besides the bending moments m_{Ed}, which affect the strains ε_v and subsequently the shear stress resistance $\tau_{Rd,c}$, the control section location may also affect the shear utilisation τ_{Ed} / $\tau_{Rd,c}$. In fact, the design shear forces v_{Ed} and bending moments m_{Ed} and m_{Rd} can be taken at a distance $d/2$ from either the support edge or the concentrated load. As such, the locations of rail traffic loads and control sections to be chosen are those leading to the greatest shear utilisations τ_{Ed} / $\tau_{Rd,c}$.

In order to present real-world case studies, all other relevant loads are also applied and factored, such as self-weight and permanent loads, as well as thermal actions and footpath loading, where applicable; nonetheless, it is the rail traffic load that affects the design shear force values the most. The material partial safety factors $\gamma_C = 1.50$ and $\gamma_S = 1.15$ are taken from EC2:2023 and are unchanged from previous Eurocode versions.

Finally, it should be emphasised that a linear elastic plate analysis is likely to overestimate shear forces at short distances from a support or concentrated load, as discussed in Section 2.1.

5.1. Eaglescliffe underbridge

Underbridge DSN1/14 at Eaglescliffe (United Kingdom) was reconstructed in 2016 to replace an older steel girder deck with timber waybeams. The bridge carries one ballasted track and its deck is a pre-

Table 2
Eaglescliffe underbridge – Main data.

Description	Value
Skew span	4.35 m
Depth	0.3 m
Right width	3.7 m
Skew angle	26.5°
Concrete strength class	C40/50
Modulus of elasticity of concrete	35.2 GPa
Poisson's ratio of concrete	0.2
Characteristic tensile strength (5% fractile)	2.46 MPa
Maximum aggregate diameter	20 mm
Nominal cover	45 mm
Steel reinforcement	B500B
Modulus of elasticity of steel	200 GPa
Longitudinal tensile reinforcement ratio (midspan)	2.16%
Longitudinal tensile reinforcement ratio (supports)	1.08%
Transverse tensile reinforcement ratio	0.61%
Minimum shear stress resistance	0.93 MPa
Number of elements	1480
Element size (typical)	0.15 x 0.15 m^2

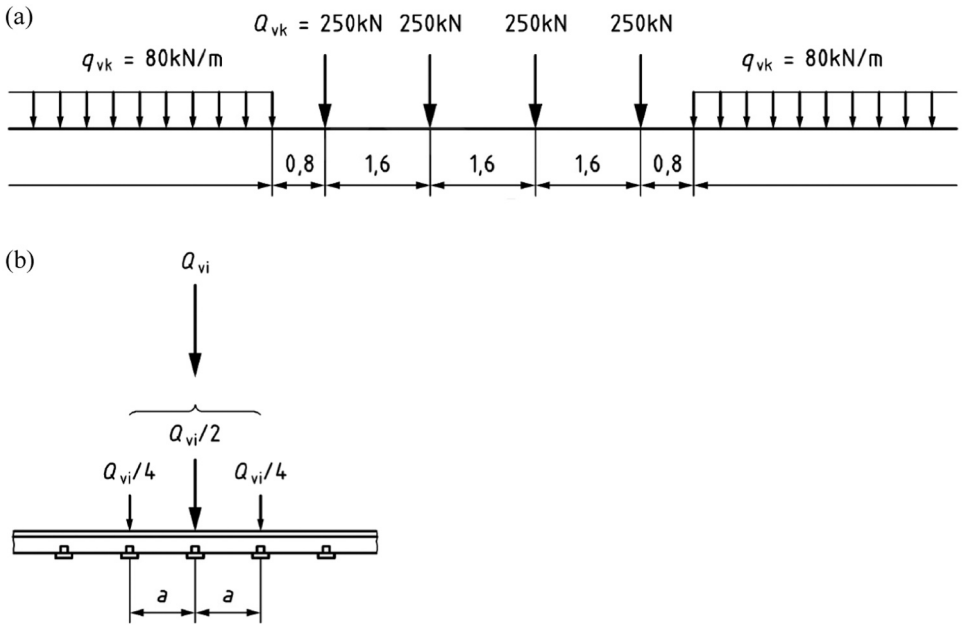

Fig. 7. Rail traffic loads: (a) Load Model 71; (b) longitudinal distribution of a point load by the rail (reprinted with permission from European Committee for Standardization [15]).

cast concrete solid slab with two upstands.

Table 2 summarises the main information on deck geometry, material properties and structural analysis. In spite of its short span, the concrete deck is quite slender, with a span-to-depth ratio of 14.5:1. The deck is supported on 10x200 mm^2 unreinforced elastomeric strips, modelled by means of distributed linear springs of stiffness 14,000 MN/m^3, so as to limit the onset of unrealistic shear forces.

Fig. 8 shows a sketch of the main flexural reinforcement of the deck, along with the locations of the LM71 point loads and the control sections. The tensile area is clearly along the bottom of the slab. The reinforcement grid is orthogonal with the longitudinal reinforcement parallel to the free edges (Arrgt. 1, Fig. 1). The largest point load $Q_{vi}/2$ is placed at 2d from the support edge, since a test has confirmed that such positioning leads to the greatest shear utilisations τ_{Ed} / $\tau_{Rd,c}$ for all verifications.

The dynamic factor φ_3 is 1.876; therefore, the design axle load Q_{vd} is 822.9 kN (Eq. 41) and the design point load $Q_{vi}/2$ is 205.7 kN (Fig. 7b).

Table 3 reports the design values of the shear forces, as well as of moments and strains concurrent with the maximum principal shear force v_{Ed}. Note that the directions of the maximum principal shear force α_v are not quite comparable to the skew angle (Table 2) but, when averaged over the control sections, they get very close to it. This confirms that the control sections can be conveniently taken parallel to the support line. In fact, performing the shear verification in a direction perpendicular to the control sections, i.e., equal to the skew angle, rather than in the direction of the principal shear force α_v, entails a small error (see also Section 2.2). This approach is particularly convenient when averaging is performed, because the directions of the principal shear force differ at each element.

Fig. 9 depicts the design shear forces in the direction perpendicular to the control sections, in which the peaks due to the point loads are quite noticeable. To smooth out the peak shear values, the principal shear forces acting over the control sections are averaged [41]. The averaging is performed over the maximum width of 2d both sides of the peak. It is worth noting that the designer/assessor may still consider only the element with the maximum principal shear force and its direction for the shear verification, thus avoiding the burden of redistribution.

Finally, the applied moments do not feature large peaks and therefore averaging is not performed. They do not lead to reinforcement yielding, as confirmed by the fairly low strain values in Table 3.

Table 3
Eaglescliffe underbridge – Design shear forces, moments and strains.

Distance of control section from concentrated load	*d*	*d/2*
Shear force along x-axis, $v_{Ed,x}$ [kN/m]	−335.8	−591.1
Shear force along y-axis, $v_{Ed,y}$ [kN/m]	−301.5	−492.3
Maximum principal shear force, v_{Ed} [kN/m]	451.3	769.3
Direction of maximum principal shear force, α_v [°]	41.92	39.79
Average principal shear force over the control section, $v_{Ed,av}$ [kN/m]	401.3	405.3
Average direction of principal shear force, $\alpha_{v,av}$ [°]	26.46	24.69
Bending moment along x-axis, $m_{Ed,x}$ [kNm/m]	53.7	86.0
Bending moment along y-axis, $m_{Ed,y}$ [kNm/m]	20.7	55.9
Twisting moment, $m_{Ed,xy}$ [kNm/m]	39.4	39.4
Moment across the control section, m_{Ed} [kNm/m]	78.6	111.5
Direction of principal moment, α_m [°]	33.6	34.5
Average moment over the control section, $m_{Ed,av}$ [kNm/m]	77.0	100.1
Effective shear span, a_{cs} [m]	0.236	0.275
Mechanical shear span, a_v [m]	0.118	0.127
Longitudinal reinforcement strain, ε_x [‰]	0.461	0.813
Transverse reinforcement strain, ε_y [‰]	0.113	0.800
Equivalent reinforcement ratio across the control section – cos^2 [%]	0.98	0.98
Equivalent reinforcement ratio across the control section – cos^4 [%]	0.72	0.72
Resisting moment across the control section, m_{Rd} [kNm/m]	216.9	216.9

5.2. Castle Mill Stream underbridge

Castle Mill Stream underbridge at Oxford (United Kingdom) was built in 2016 to replace an older three-span steel lattice girder deck. The new deck is a tapered continuous shear-key deck with two upstands and carries four ballasted tracks.

Table 4 summarises the main information on deck geometry, material properties and structural analysis. The deck is supported by 80 laminated elastomeric bearings, which are modelled by means of point linear springs of stiffness variable from 1220 to 2570 MN/m.

Fig. 10 shows a sketch of the main flexural reinforcement of half the deck, along with the locations of the LM71 point loads and the control sections. The greatest shear forces are found in proximity of the intermediate support and the tensile area is obviously on the topside of the slab. Also here, the reinforcement grid is orthogonal with the longitudinal reinforcement parallel to the free edges (Arrgt. 1, Fig. 1). The largest point load $Q_{vi}/2$ is located at 2d from the support edge, since a test has confirmed that such positioning leads to the largest shear utilisations τ_{Ed} / $\tau_{Rd,c}$ for all verifications.

The dynamic factor φ_3 is 1.413; therefore Q_{vd} = 619.8 kN (Eq. 41) and the design point load $Q_{vi}/2$ is 154.9 kN (Fig. 7b).

In continuous bridges, the load model SW/0 should also be considered [15]. The load model SW/0 consists of uniformly distributed loads only and is globally heavier than the LM71; however, it is not considered further because the shear design of the deck is governed by the LM71.

Table 5 reports the design values of the shear forces, as well as moments and strains concurrent with the maximum principal shear force v_{Ed}. The direction of the principal shear force α_v is very close to the skew angle (Table 4). Since shear forces and moments along the control sections do not feature large peaks, averaging is not performed and the shear verification is conveniently carried out considering only the element with the maximum principal shear force and its direction.

Since $v_{Ed,y}$ / $v_{Ed,x}$ = 0.25 and 0.24 at the control sections d and $d/2$,

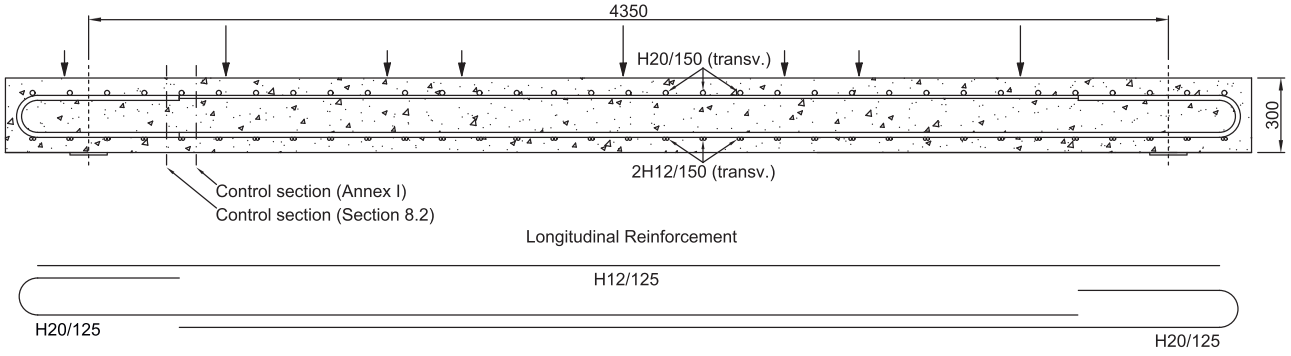

Fig. 8. Eaglescliffe underbridge: flexural reinforcement of deck with illustrative locations of point loads and control sections [mm].

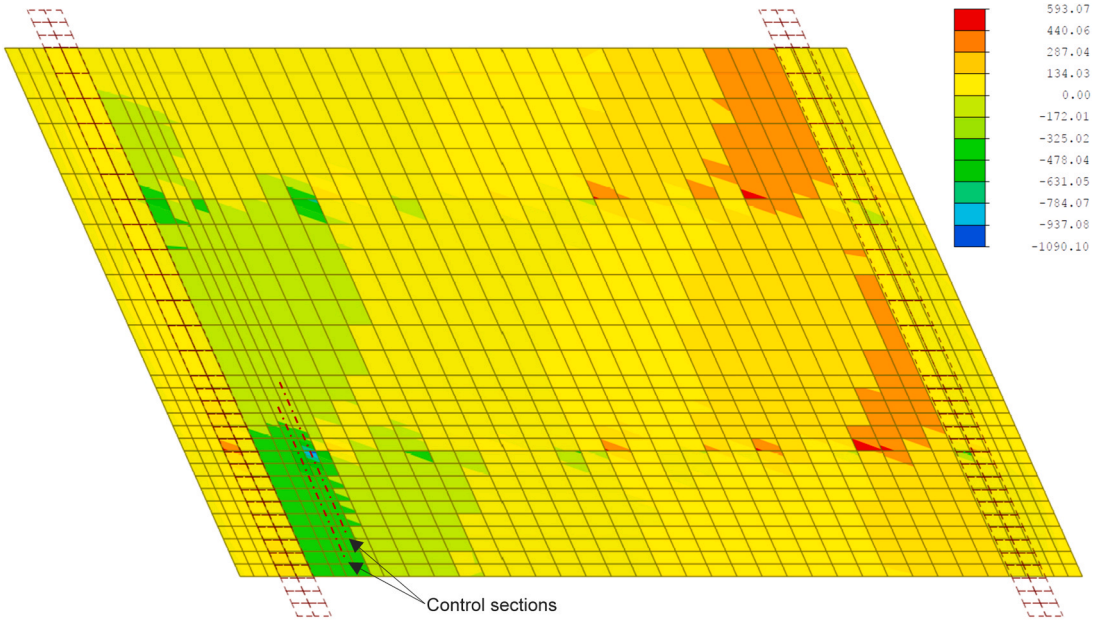

Fig. 9. Design shear forces in the direction perpendicular to the control sections (θ = 26.5°) [kN/m] (area below upstands not shown).

Table 4
Castle Mill Stream underbridge – Main data.

Description	Value
Skew span	8.715 m
Depth	0.475–0.575 m
Right width	16.1 m
Skew angle	−14.6°
Concrete strength class (beams)	C50/60
Modulus of elasticity of concrete (beams)	37.3 GPa
Concrete strength class (shear keys)	C90/105
Modulus of elasticity of concrete (shear keys)	43.6 GPa
Poisson's ratio of concrete	0.2
Characteristic tensile strength (5% fractile, beams)	2.85 MPa
Maximum aggregate diameter (beams)	20 mm
Nominal cover	40 mm
Steel reinforcement	B500B
Modulus of elasticity of steel	200 GPa
Longitudinal tensile reinforcement ratio (end support)	0.61%
Longitudinal tensile reinforcement ratio (intermediate support)	1.67%
Transverse tensile reinforcement ratio	0.33%
Minimum shear stress resistance	0.74 MPa
Number of elements	3604
Element size (typical)	0.54x0.48 m^2

respectively, the slab may be designed as straight, by using the effective depth d_x, the reinforcement ratio ρ_x, as well as the design shear force along the x-axis $v_{Ed,x}$ (Eq. 32). Nonetheless, such as a simplification is not applied in the following and the proposed procedures are applied in full.

Fig. 11 depicts the design shear forces in the direction of the principal shear force α_v = -13.63°. Since there are distributed loads pushing

Table 5
Castle Mill Stream underbridge – Design shear forces, moments and strains.

Distance of control section from support edge	*d*	*d/2*
Shear force along x-axis, $v_{Ed,x}$ [kN/m]	750.2	795.7
Shear force along y-axis, $v_{Ed,y}$ [kN/m]	−190.5	−193.0
Maximum principal shear force, v_{Ed} [kN/m]	774.0	818.8
Direction of maximum principal shear force, α_v [°]	−14.25	−13.63
Bending moment along x-axis, $m_{Ed,x}$ [kNm/m]	−533.6	−729.4
Bending moment along y-axis, $m_{Ed,y}$ [kNm/m]	−52.5	−98.5
Twisting moment, $m_{Ed,xy}$ [kNm/m]	−44.6	−14.0
Moment along the direction of the principal shear force, m_{Ed} [kNm/m]	−483.4	−688.1
Direction of principal moment, α_m [°]	5.3	1.3
Effective shear span, a_{cs} [m]	0.624	0.840
Mechanical shear span, a_v [m]	0.270	0.315
Longitudinal reinforcement strain, ε_x [‰]	0.822	1.113
Transverse reinforcement strain, ε_y [‰]	0.356	0.663
Equivalent reinforcement ratio along the direction of the principal shear force – $\cos^2$ [%]	1.60	1.59
Equivalent reinforcement ratio along the direction of the principal shear force – $\cos^4$ [%]	1.49	1.49
Resisting moment along the direction of the principal shear force, m_{Rd} [kNm/m]	−1357	−1375

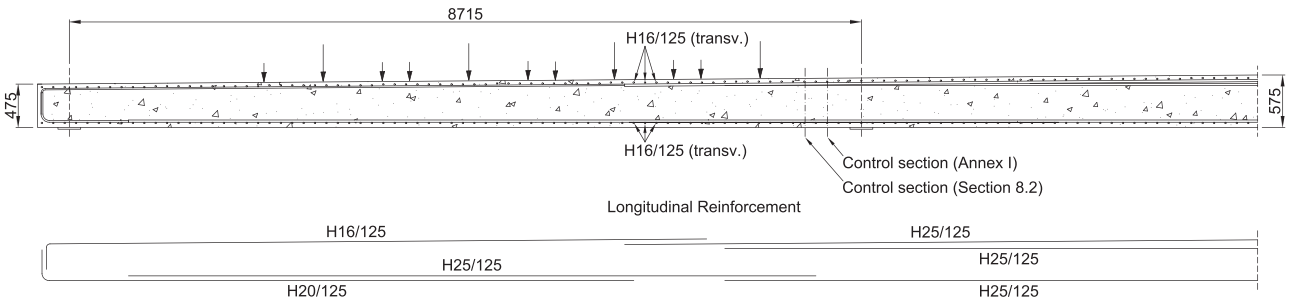

Fig. 10. Castle Mill Stream underbridge: flexural reinforcement of half deck with illustrative locations of point loads and control sections [mm].

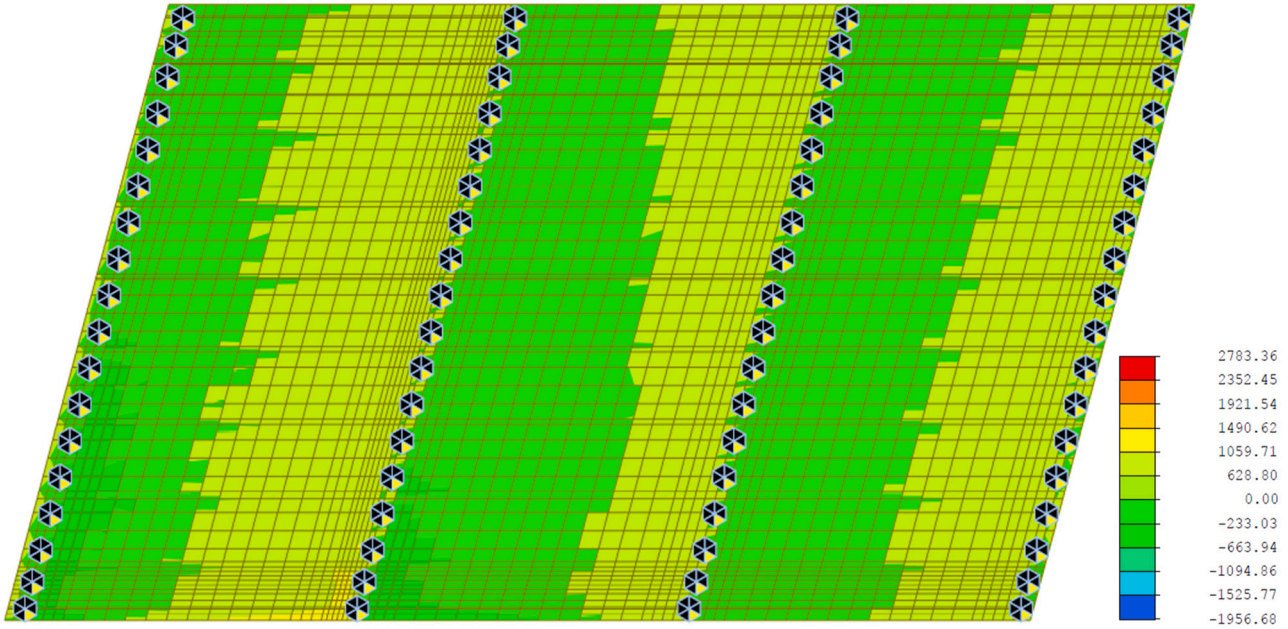

Fig. 11. Design shear forces in the direction of the principal shear force α_v = -13.63° [kN/m] (area below upstands not shown).

against the slab on the tension side, the design shear force may be reduced according to EC2:2023 (see Section 3.2). However, given the predominance of the concentrated loads over the distributed loads on the design shear forces, this reduction is disregarded.

Finally, the relatively high values of the hogging moment m_{Ed}, due to the proximity to the intermediate supports, do not lead to reinforcement yielding, as the resisting moments m_{Rd} are much greater. This is confirmed by the moderate reinforcement strain values in Table 4.

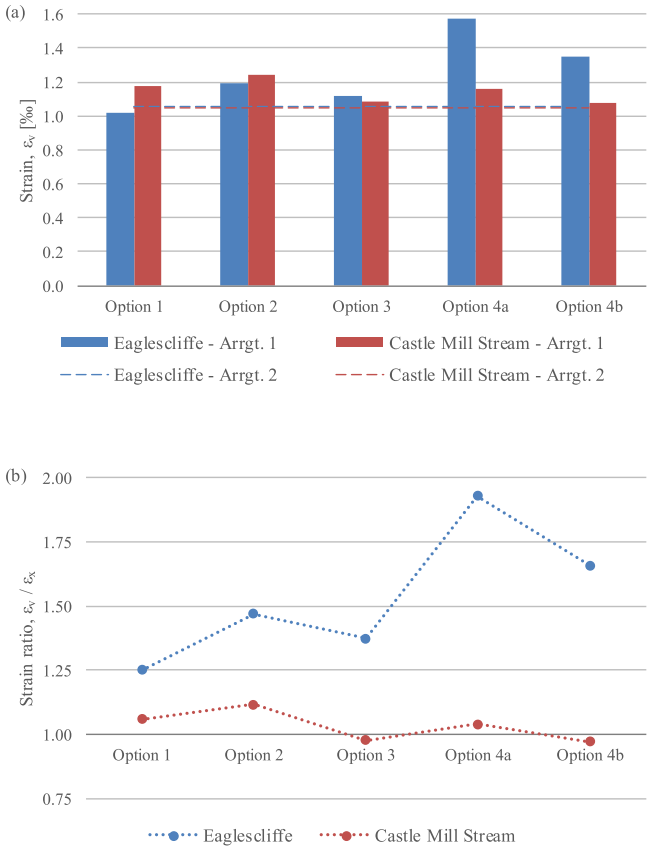

Fig. 12. Comparison of proposed calculation options: (a) strain (Arrgt. 1 & 2); (b) strain ratio (Arrgt. 1).

5.3. Results

Fig. 12a shows the strains calculated with the options proposed in Section 4.3.1 for the two decks. It also shows the strains calculated with the reinforcement grid rotated by the skew angle, i.e., with the same reinforcement but placed according to Arrgt. 2 (Fig. 1). As such, the longitudinal reinforcement becomes perpendicular to the support line, thus minimising the deviation of the principal shear force from the main reinforcement. Since this is the case implicitly considered in the EC2:2023 formulations, the strain values do not depend on the proposed calculation options. Incidentally, the strains for the two decks with Arrgt. 2 happen to have nearly the same value. Also, the strains with Arrgt. 1 are generally greater than those calculated with Arrgt. 2, as expected.

As discussed in Section 4.3.1, Option 4b calculates also the strains in the *t*-direction ε_t under the usual assumption of ignoring the concrete tensile strength. Such strains result in 0.671‰ and 1.130‰ for Eaglescliffe and Castle Mill Stream, respectively, leading to $\varepsilon_t / \varepsilon_v = 0.427$ and 0.978. In the following, Option 4b is taken as benchmark.

For Eaglescliffe ($\mu = 0.60$), Options 1–3 tend to grossly underestimate strains, whereas Option 4a is greater than Option 4b (+16.3%). This is expected as Option 4a has been shown to be the safest method (Section 4.3.2). Fig. 12b shows that the strains ε_v are much larger than those in the longitudinal reinforcement ε_x, mainly due to the deck significant skew angle. On the other hand, for Castle Mill Stream ($\mu = 0.20$), Options 1 and 2 significantly overestimate the strains ε_v (up to +15.1% compared with Option 4b), whereas Options 3 and 4a much less so (+0.7% and +7.0%, respectively). As can be seen in Fig. 12b, the strains ε_v are comparable to the reinforcement strain ε_x, with Options 3 and 4 returning values very close to ε_x, due to the small skew angle.

Fig. 13 shows the shear stress resistances $\tau_{Rd,c}$ calculated with EC2:2023, including the verification of Section 8.2, which does not involve strains. The shear stress resistances calculated with the rotated reinforcement arrangement are also depicted (Arrgt. 2, Fig. 1).

Firstly, for the Section 8.2 verification, it can be noticed that the use of the mechanical shear span a_v in lieu of the effective depth d increases $\tau_{Rd,c}$, namely by 4.3% for Eaglescliffe and as much as 20.1% for Castle

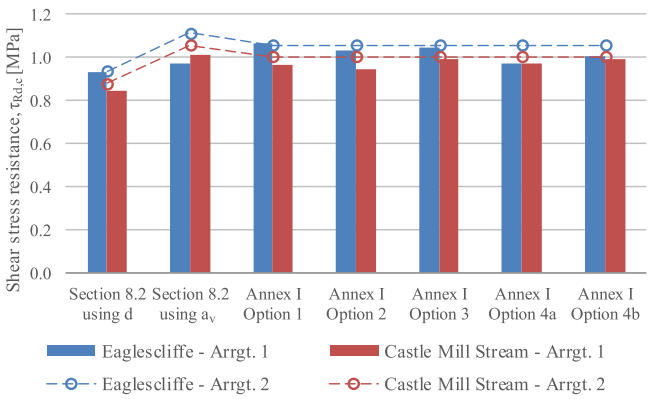

Fig. 13. Comparison of shear stress resistances calculated with EC2:2023.

Mill Stream. Then, for the Annex I verification, it can be seen that the variations between the different strain calculation options reduce when considering their effects on the shear stress resistance. For Eaglescliffe, the refined verification of Annex I further increases $\tau_{Rd,c}$, up to 9.4%, compared with the calculation of EC2:2023 Section 8.2 using a_v. In contrast, for Castle Mill Stream, the more complex refined verification does not improve the Section 8.2 resistance when using a_v: indeed, the smallest reduction is given by Option 4b (-2.0%). Furthermore, when considering Arrgt. 2, the Section 8.2 verification using a_v expectedly increases $\tau_{Rd,c}$ for both decks, but the refined strain-based verification leads to slightly lower $\tau_{Rd,c}$ values than those calculated using a_v.

Fig. 14 shows the shear resistances $v_{Rd,c}$ calculated with both EC2–1:2004 and EC2:2023. The new EC2:2023 Section 8.2 verification using the effective depth d leads to a greater shear resistance $v_{Rd,c}$ than EC2–1:2004 only for Eaglescliffe. In contrast, when using the mechanical shear span a_v, the Section 8.2 verification leads to greater shear resistances than EC2–1:2004 for both decks (+22.0% for Eaglescliffe, +7.5% for Castle Mill Stream), which accords with the findings of Díaz-Pavón et al. [10]. The other values reflect the points previously made about the shear stress resistance $\tau_{Rd,c}$.

Finally, it is noted that both decks required shear reinforcement, regardless of the Eurocode 2 formulation used, due to their slenderness and large design shear forces.

6. Recommendations on the shear design and assessment of skew slabs

Based on the case studies and numerical investigations presented above, the following remarks and recommendations can be made for applying the shear provisions of EC2:2023 to the design or assessment of significantly skewed slabs.

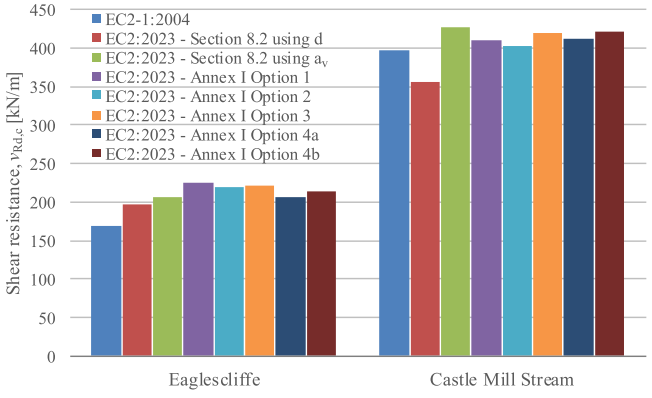

Fig. 14. Comparison of shear resistances calculated with EC2–1:2004 and EC2:2023.

- The standard formulation of EC2:2023 Section 8.2 leads to greater design resistances than EC2–1:2004 when using the mechanical shear span a_v in lieu of the effective depth d. In fact, using d leads to a greater resistance only in one of the two case studies. Therefore, it is strongly advisable to use a_v whenever applicable, even though this may require some iterations in the design process. The refined verification according to EC2:2023 Annex I does not necessarily increase the shear resistance further.
- When the direction of the principal shear force significantly deviates from that of the main reinforcement, like in Arrgt. 1 and 3 (Fig. 1), an equivalent reinforcement area in the direction of the principal shear force should be computed. This can be done by applying a $\cos^4$ function to resolve the reinforcement areas in the direction of the principal shear force. Notably, the indications given in this study about the computation of the equivalent reinforcement area can be applied also to non-orthogonal reinforcement grids (Arrgt. 3, Fig. 1), which are not considered in EC2:2023.
- EC2:2023 allows simplifications when the ratio of the design shear forces $v_{Ed,y}$ / $v_{Ed,x}$ is lower than 0.5 or greater than 2. Adopting the modified thresholds of 0.25 and 4, as proposed in Eq. (32), is recommended to avoid treating significantly skewed bridges as straight.
- The refined verification according to EC2:2023 Annex I requires the computation of the strain at the level of the reinforcement in the direction of the principal shear force ε_v. Unlike the EC2:2023 Section 8.2 verification, the control section is located at $d/2$ from a support, concentrated load or discontinuity. At such short distances a FEM-based analysis may well exhibit undesired singularities; therefore, it is crucial to model supports and concentrated loads as realistically as possible, e.g., by distributing their effects over a suitable area. Then, the strain calculation is straightforward when the reinforcement does not significantly deviate from the direction of the principal shear force, like in Arrgt. 2 (Fig. 1). Otherwise, the strain on a direction along which no reinforcement is placed must be found and no indications are given in EC2:2023 in these regards. Therefore, five options of different complexity, based on the elastic behaviour of the reinforcement, are proposed to calculate the required strain. In detail:
  - Options 1 and 2, the latter based on the Swiss Code SIA 262 [43], simply amplify the strain in the longitudinal reinforcement. As such, they do not depend on the amount of transverse reinforcement, which generally has a significant influence on strains. These options may be conservative or not, so their use is not recommended, particularly with significant twisting moments, which are not unusual in skew slabs.
  - Option 3 is based on the bending utilisation, as suggested in the Swiss Code SIA 262 when the flexural reinforcement remains elastic [43]. The case studies show that, although it generally performs better than Options 1 and 2, the results are close to the most accurate Options 4 only for the less skewed deck.
  - Options 4 are based on the analytical computation of strains by using an equivalent reinforcement area. Option 4a applies a $\cos^4$ function to resolve the reinforcement areas into an equivalent reinforcement area. It is reasonably accurate when the strains in the t-direction ε_t are much smaller than the strains in the n-direction ε_n, i.e., $\varepsilon_t / \varepsilon_n \approx 0$, which may occur when the slab is cracked only perpendicularly to n [5]. In any case, using Option 4a is on the safe side. When a greater accuracy is desired and strains in the t-direction are significant ($\varepsilon_t / \varepsilon_n > 0$), Option 4b refines the results of Option 4a by calculating first the strains ε_t and then a refined equivalent reinforcement area.

It must be emphasised that the recommendations above are based on the numerical investigation and the case studies presented here. For instance, this study assumes the elastic behaviour of the reinforcement under the shear design load case, as is typical in simply supported slabs. Cases when the reinforcement is yielding under the shear design load

case, which may occur in clamped slabs, are not considered here.

In general, more experimental research is needed on the shear resistance of skew slabs to fully validate the numerical results available in literature. For instance, the experiments carried out by Cope et al. [8] showed little difference in the shear failure load between Arrgt. 1 and Arrgt. 2 (Fig. 1) [6], whereas the case studies presented here suggest a noticeable difference.

7. Conclusions

Reinforced concrete slabs are widely used in construction. Skew slabs are common in bridge decks, as they generally adapt to site constraints better than straight slabs.

While the principles underlying flexural behaviour of slabs are well understood, their shear behaviour is still under debate. The second generation of Eurocode 2, EN 1992–1–1:2023, has considerably advanced the formulation of the shear resistance without shear reinforcement. However, it still does not offer provisions readily applicable to skew slabs.

This study reviews the provisions of the first and second generation of Eurocode 2, as well as relevant research, on the shear design of concrete skew slabs without shear reinforcement. The second generation of Eurocode 2 allows for two verification levels: the standard verification in Section 8.2, to be used mainly for design, and the refined strain-based verification in the informative Annex I for assessment.

Procedures to extend the shear provisions of Eurocode 2 to skew slabs are presented, including the case of non-orthogonal reinforcement grids. More restrictive thresholds than those introduced in the new Eurocode 2 to simplify calculations are proposed.

For the refined verification, the required strain is not straightforward to compute when the direction of the principal shear force significantly deviates from that of the main reinforcement – a common case in skew slabs. Therefore, five options of different complexity for calculating the required strain are proposed and tested.

The procedures are applied to two skew railway bridge decks – one simply supported and the other continuous. In both decks, the reinforcement grids are orthogonal with the longitudinal reinforcement parallel to the free edges, so that the direction of the principal shear force deviates significantly from that of the longitudinal reinforcement.

It is found that the second generation of Eurocode 2 returns greater shear resistances than the first generation when using the mechanical shear span in lieu of the effective depth. However, the new refined strain-based verification does not necessarily improve the shear resistances calculated with the standard verification, despite its increased complexity. Furthermore, the variability exhibited by the different strain calculation options is partially reduced when considering their effects on the shear resistance. Among the options proposed for the strain calculation, it is advisable to prefer those based on the analytical calculation of strains using an equivalent reinforcement area.

Funding

No specific funding has been received for this work.

Declaration of Competing Interest

The author declares that he has no known competing financial interests or personal relationships that could have appeared to influence the work reported in this paper.

Acknowledgements

The author wishes to thank Systra UK (formerly TSP Projects) for providing the case studies and Dr Giordano Lipari for linguistic advice.

References

[1] American Association of State Highway and Transportation Officials. AASHTO LRFD Bridge Design Specifications. Eighth ed. Washington: American Association of State Highway and Transportation Officials; 2017.
[2] BSI 1990. Steel, concrete and composite bridges. Part 4: Code of practice for design of concrete bridges. BSI.
[3] BSI 2007. UK National Annex to Eurocode 2: Design of concrete structures. Part 2: Concrete bridges - Design and detailing rules. BSI.
[4] Cavagnis F, Fernández Ruiz M, Muttoni A. A mechanical model for failures in shear of members without transverse reinforcement based on development of a critical shear crack. Eng Struct 2018;157:300–15.
[5] Clark LA. Concrete bridge design to BS 5400. London and New York: Construction Press; 1983.
[6] Cope RJ. Flexural shear failure of reinforced concrete slab bridges. Proc Inst Civ Eng, Part 1985;2(79):559–83.
[7] Cope RJ, Clark LA. *Concrete Slabs: Analysis and Design* London. Elsevier Applied Science Publishers; 1984.
[8] Cope RJ, Rao PV, Edwards KR. Shear in skew reinforced concrete slab bridges. University of Liverpool; 1983.
[9] Denton S, Shave J, Bennetts J, Hendy C. Design of concrete slab elements in biaxial bending. In: Denton S, editor. Bridge Design to Eurocodes - UK Implementation, 22-23 November 2010 London. London: ICE Publishing; 2011. p. 250–69.
[10] Díaz-Pavón E, Rodríguez R, Ley J, López P. Contributions of the future Eurocode 2 for assessment of existing concrete structures. Hormigón y Acero 2023;74:139–50.
[11] European Committee for Standardization. Eurocode 2: Design of concrete structures. *Part 1-1: General rules and rules for building*. Brussels: CEN; 2004.
[12] European Committee for Standardization. Eurocode 2: Design of concrete structures. *Part 2: Concrete Bridges - Design and detailing rules*. Brussels: CEN; 2005.
[13] European Committee for Standardization. Concrete - Specification, performance, production and conformity. Brussels: CEN; 2021.
[14] European Committee for Standardization. Eurocode 2 - Design of concrete structures. *Part 1-1: General rules and rules for building, bridges and civil engineering structures*. Brussels: CEN; 2023.
[15] European Committee for Standardization. Eurocode 1 - Actions on structures. Part 2: Traffic loads on bridges and other civil engineering works. Brussels: CEN; 2023.
[16] Henze L, Rombach GA, Harter M. New approach for shear design of reinforced concrete slabs under concentrated loads based on tests and statistical analysis. Eng Struct 2020:219.
[17] Hillerborg, A. A Plastic Theory for the Design of Reinforced Concrete Slabs. 6th IABSE Conference, 1960 Stockholm. 178-186.
[18] Hulsebosch CJF. Skewed slab highway bridges (MSc). Delft University of Technology; 2019.
[19] International Federation for Concrete Structures. fib Model Code for Concrete Structures 2010. Berlin: Wilhelm Ernst & Sohn; 2013.
[20] International Federation for Concrete Structures 2023. fib Model Code for Concrete Structures (2020). Lausanne: International Federation for Sructural Concrete (fib).
[21] Jaeger T, Marti P. Reinforced concrete slab shear prediction competition: entries and discussion. Acids Struct J 2009;106:309–18.
[22] Jofriet JC, McNeice GM. Finite element analysis of reinforced concrete slabs. J Struct Div 1971;97:785–806.
[23] Johansen KW. Yield-line Formulae for Slabs. CRC Press; 1972.
[24] Lantsoght EOL, De Boer A, Van Der Veen C. Distribution of peak shear stress in finite element models of reinforced concrete slabs. Eng Struct 2017;148:571–83.
[25] Lantsoght EOL, Van Der Veen C, De Boer A, Walraven JC. Influence of width on shear capacity of reinforced concrete members. Acids Struct J 2014;111:1441–50.
[26] Lantsoght EOL, Van Der Veen C, Walraven JC, De Boer A. Recommendations for the shear assessment of reinforced concrete slab bridges from experiments. Struct Eng Int 2013;4:418–26.
[27] Lantsoght EOL, Yang Y, Van Der Veen C, De Boer A, Hordijk DA. Ruytenschildt bridge: field and laboratory testing. Eng Struct 2016;128:111–23.
[28] Lenschow RJ, Sozen MA. A yield criterion for reinforced concrete under biaxal moments and forces. Structural Research Series. University of Illinois; 1966.
[29] Lipari A. A comparative study of shear design methods for straight and skew concrete slabs. Eng Struct 2020;208:1–16.
[30] Marti P. Design of concrete slabs for transverse shear. Acids Struct J 1990;87:180–90.
[31] Midas Information Technology Co., Midas Civil online manual [Online]. Available: ⟨http://manual.midasuser.com/EN_Common/Civil/945/index.htm⟩ [Accessed 10 April 2025].
[32] Miguel PF, Fernández MA, Hegger J, Schmidt M. Shear resistance of members without shear reinforcement in presence of compressive axial force in the next Eurocode 2. Hormigón y Acero 2023;74:41–60.
[33] Miller RA, Aktan AE, Shahrooz BM. Destructive testing of decommissioned concrete slab bridge. J Struct Eng 1994;120:2176–98.
[34] Morrison DG, Weich GR. Free-edge and obtuse-corner shear in R/C skew bridge decks. Acids Struct J 1987;84:3–9.
[35] Moya L, Lantsoght EOL. Parametric Study on the Applicability of AASHTO LRFD for Simply Supported Reinforced Concrete Skewed Slab Bridges. Infrastructures 2021:6.
[36] Muttoni, A. 2023. Background document to clauses 4.3.3 and Annex A - Partial safety factors for materials. Background Document for FprEN 1992-1-1. CEN.
[37] Muttoni A, Fernández Ruiz M. Shear strength of members without transverse reinforcement as function of critical shear crack width. Acids Struct J 2008;105:163–72.

[38] Muttoni, A., Fernández Ruiz, M., Cavagnis, F. & Simões, J.T. 2023. Background document to clauses 8.2.1 and 8.2.2 - Shear in members without shear reinforcement. Background Document for FprEN 1992-1-1. CEN.
[39] Natário F, Fernández Ruiz M, Muttoni A. Shear strength of RC slabs under concentrated loads near clamped linear supports. Eng Struct 2014;76:10–23.
[40] OBrien EJ, Keogh DL, O'Connor AJ. Bridge Deck Analysis. Second ed. Boca Raton: CRC Press; 2015.
[41] Pacoste C, Plos M, Johansson M. Recommendations for finite element analysis for the design of reinforced concrete slabs. Stockholm: KTH; 2012.
[42] Rombach GA. Finite-element Design of Concrete Structures: Practical problems and their solutions. London: ICE Publishing; 2011.
[43] SIA 2013. Betonbau. Zurich: Schweizerischer Ingenieur- und Arkitektenverein.
[44] Théoret P, Massiccotte B, Conciatori D. Analysis and design of straight and skewed slab bridges. J Bridge Eng 2012;17:289–301.
[45] Vaz Rodrigues R. Shear strength of reinforced concrete bridge deck slabs (PhD). École Polytechnique Fédérale de Lausanne; 2007.
[46] Wood RH, Armer GST. The theory of the strip method for design of slabs. Proc Inst Civ Eng 1968;41:285–311.